SOLUTION-PROCESSABLE ROD-SHAPED MOLECULAR SEMICONDUCTORS AND FIELD-EFFECT TRANSISTOR APPLICATIONS

A Master's Thesis

By

İbrahim DENEME

August 2018

ABDULLAH GÜL UNIVERSITY

İbrahim DENEME
SOLUTION-PROCESSABLE ROD-SHAPED MOLECULAR SEMICONDUCTORS AND FIELD-EFFECT TRANSISTOR APPLICATIONS
AGU 2018

SOLUTION-PROCESSABLE ROD-SHAPED MOLECULAR SEMICONDUCTORS AND FIELD-EFFECT TRANSISTOR APPLICATIONS

A THESIS
SUBMITTED TO THE DEPARTMENT OF ADVANCED MATERIALS AND NANOTECHNOLOGY AND THE GRADUATE SCHOOL OF ENGINEERING AND SCIENCES OF ABDULLAH GÜL UNIVERSITY
IN PARTIAL FULFILLMENT OF THE REQUIREMENTS
FOR THE DEGREE OF
MASTER OF SCIENCE

By
İbrahim DENEME
August 2018

SCIENTIFIC ETHICS COMPLIANCE

I hereby declare that all information in this document has been obtained in accordance with academic rules and ethical conduct. I also declare that, as required by these rules and conduct, I have fully cited and referenced all materials and results that are not original to this work.

İbrahim DENEME

REGULATORY COMPLIANCE

M.Sc. thesis titled "Solution-Processable Rod-Shaped Molecular Semiconductors and Field-Effect Transistor Applications" has been prepared in accordance with the Thesis Writing Guidelines of the Abdullah Gül University, Graduate School of Engineering and Science.

Prepared By

İbrahim DENEME

Advisor

Assoc. Prof. Hakan USTA

Head of the Advanced Materials and Nanotechnology Program

Prof. Murat DURANDURDU

ACCEPTANCE AND APPROVAL

M.Sc. thesis titled "Solution-Processable Rod-Shaped Molecular Semiconductors and Field-Effect Transistor Applications" was prepared by İbrahim DENEME, which has been accepted by the jury in the Advanced Materials and Nanotechnology Graduate Program at Abdullah Gül University, Graduate School of Engineering and Science.

31/08/2018

JURY:

Advisor	: Assoc. Prof. Hakan USTA
Member	: Assoc. Prof. Evren MUTLUGÜN
Member	: Assoc. Prof. M. Serdar ÖNSES

APPROVAL:

The acceptance of this M.Sc. thesis has been approved by the decision of the Abdullah Gül University, Graduate School of Engineering and Science, Executive Board dated ….. /….. / …….. and numbered ……..……. .

Graduate School Dean
Prof. İrfan ALAN

ABSTRACT

SOLUTION-PROCESSABLE ROD-SHAPED MOLECULAR SEMICONDUCTORS AND FIELD-EFFECT TRANSISTOR APPLICATIONS

İbrahim DENEME

M.Sc. in Advanced Materials and Nanotechnology

Supervisor: Assoc. Prof. Hakan USTA

August 2018

The structural design and synthetic development of novel *n*-channel organic semiconductors have attracted considerable scientific and technological attention in order to understand the fundamentals of charge-transport mechanisms in organic (opto)electronics. Although large number of *n*-channel semiconductors have been reported in the literature over the past few decades, solution-processable and air-stable *n*-channel semiconductors are still scarce. Herein, we report the design, synthesis, single crystal structures, optoelectronic properties, solution-processed thin-film morphologies/microstructures, and organic field effect characteristics of two molecular indeno[1,2-b]fluorenes containing (triisopropylsilyl)ethynyl groups in the 2,8-positions functionalized with carbonyl and dicyanovinylene moieties in the 6,12-positions. Inclusion of electron-withdrawing carbonyl, dicyanovinylene, and (triisopropylsilyl)ethynyl groups to indeno[1,2-b]fluorene cores create fully acceptor type π-conjugated structures, 2,8-(triisopropylsilyl)ethynyl-indeno[1,2-b]fluorine-6,12-diones (TIPS-IFDK) and 2,8-(triisopropylsilyl)ethynyl-indeno [1,2-b]fluorine-6,12-bis(dicyanoviynlene) (TIPS-IFDM). HOMO/LUMO energies of the new compounds are -5.77/-3.65 eV and -5.84/-4.18 eV for TIPS-IFDK and TIPS-IFDM, respectively. Slightly increased optical band gaps of 2.12 eV (for TIPS-IFDK) and 1.66 eV (for TIPS-IFDM) compared to previously developed donor-acceptor type indenofluorenes could be attributable to their acceptor type π-conjugated structures. Solid-state

arrangements and intermolecular π-π interactions of TIPS-IFDK and TIPS-IFDM were examined via single single-crystal X-ray diffraction (XRD) analysis. The new semiconductors exhibited 1-D columns in the solid-state. OFETs in top-contact/bottom-gate transistor geometry utilizing TIPS-IFDM semiconductor layer fabricated via solution-shearing possessed *n*-channel charge transporting characteristics with an air-stable electron mobility 0.02 $cm^2 (V\ s)^{-1}$ and I_{on}/I_{off} ratios of 10^7. However, TIPS-IFDK exhibited three orders of magnitude lower electron mobility in OFETs because of less effective π-π interactions and the poor crystallinity in thin-film phase, and TIPS-IFDK based OFETs did not exhibit ambient stability. Electronic effects of (trialkylsilyl)ethynyl grops substitutions on frontier molecular orbitals were reavealed by DFT calculations. To the best of our knowledge, TIPS-IFDM is the first example of a solution-processable, air-stable *n*-type molecular semiconductor functionalized with (trialkylsilyl)ethynyl groups along the long molecular axis.

Our results clearly provide a novel molecular design approach for the development of easily synthesizable, solution-processable semiconductors for ambient-stable *n*-channel organic field-effect transistors and potentially various organic (opto)electronic technologies.

Keywords: Solution-Processable, Air-Stable, N-Channel, Organic Semiconductor

ÖZET

SOLÜSYONDAN PROSES EDİLEBİLİR ÇUBUK YAPISINDA MOLEKÜLER YARI-İLETKENLER VE ALAN ETKİLİ TRANSİSTÖR UYGULAMALARI

İbrahim DENEME
İleri Malzemeler ve Nanoteknoloji Anabilim Dalı Yüksek Lisans
Tez Yöneticisi: Doç. Dr. Hakan USTA

Ağustos 2018

Yeni *n*-tipi yarı iletkenlerin yapısal dizaynı ve sentetik olarak geliştirilmesi yük taşıma mekanizmasının temellerinin anlaşılması noktasında bilimsel ve teknolojik alanlarda önemli derecede ilgi uyandırmıştır. Son yıllarda literatürde mevcut çok sayıda *n*-tipi yarı iletken olmasına rağmen, solüsyondan proses edilebilen ve havada kararlı *n*-tipi yarı-iletken malzeme sayısı oldukça sınırlıdır. Burada biz, indeno[1,2-b]floren ve (triizopropilsilil)etinil tabanlı, 6,12-pozisyonlarında disiyanovinilen ve 2,8-pozisyonlarında ise karbonil fonksiyonel grupları içeren iki yeni moleküler yarı-iletkenlerin dizaynı, sentezi, tek kristal yapıları, optoelektronik özellikleri, çözelti ile proses edilmiş ince-film morfolojilerini/mikroyapılarını ve organik alan etkili transistör uygulamalarını ortaya koyduk. Elektron çekici karbonil, disiyanovinilen ve (triizopropilsilil)etinil gruplarının indeno[1,2-b]floren π-merkezine dahil edilmesi, tamamen akseptör tipinde π-konjuge yapının oluşmasına sebep olmaktadır. Söz konusu yeni moleküller, 2,8- (triizopropilsilil)etinil-indeno[1,2-b]floren-6,12-dion (TIPS-IFDK) ve 2,8-(triizopropilsilil)etinil-indeno[1,2-b]floren-6,12-bis(disiyanoviinilen) (TIPS-IFDM)'dir. Yeni bileşiklerin HOMO/LUMO enerjileri sırasıyla TIPS-IFDK için -5.77 / -3.65 eV ve TIPS-IFDM için -5.84 / -4.18 eV'dir. Daha önce geliştirilen donör-akseptör tipi indenofluorenler ile kıyaslandığında tamamen akseptör yapıda π-konjuge sisteme sahip oldukları için yeni moleküllerin optik bant aralıklarında artış gözlemlenmiştir. (TIPS-IFDK için 2.12 eV ve TIPS-IFDM için 1.66 eV) TIPS-IFDK ve TIPS-IFDM

yarı-iletkenlerinin katı-hal düzenlemeleri ve moleküller arası π-π etkileşimleri, tek kristal X-ray difraksiyon (XRD) analizi ile incelenmiştir. Söz konusu yarı-iletkenler katı halde 1-D kolon yapısı ortaya koymuştur. Bu tez kapsamında geliştirilen TIPS-IFDM yarı-iletkeni kullanılarak, solüsyon-makaslama (solution-shearing) yöntemi ile alt kapı/üst temas organik alan etkili transistörler üretilmiştir. Havada son derece kararlı olan söz konusu transistörler *n*-tipi yük taşıma karakterinde olup, 0.02 cm^2/Vs elektron hareketliliği, 10^7 I_{on}/I_{off} oranı sergilemiştir. Buna rağmen bu tez kapsamında geliştirilen diğer molekül TIPS-IFDK, TIPS-IFDM ile kıyaslandığında 10^3 kat daha az elektron hareketliliği ortaya koymuştur. Bu durum TIPS-IFDK molekülünün zayıf π-π etkileşimleri ve ince-film fazında zayıf kristal yapısından kaynaklanmaktadır. Dolayısıyla TIPS-IFDK tabanlı OFET'ler havada kararlı değildir. (trialkilsilil)etinil grubunun HOMO/LUMO orbitalleri üzerindeki elektronik etkileri DFT hesaplamaları ile ortaya çıkarıldı. Bildiğimiz kadarıyla, TIPS-IFDM, uzun moleküler eksen (x) boyunca (trialkilsilil) etinil gruplarıyla fonksiyonel hale getirilmiş, çözücüde proses edilebilen, havada kararlı, *n*-tipi moleküler yarı iletkenlerin ilk örneğidir. Elde ettiğimiz sonuçlar, havada kararlı *n*-tipi organik alan etkili transistörler ve çeşitli organik optoelektronik teknoloji uygulamaları için kolay sentezlenebilir, solüsyondan proses edilebilir yeni molekülerin nasıl dizayn edileceği noktasında önemli bilgiler vermektedir. Bu alanlarda ilerde yapılacak araştırmalara ışık tutmaktadır.

Anahtar kelimeler: Solüsyondan Proses Edilebilen, Havada Kararlı, , N-tipi, Organik Yarı İletkenler

Acknowledgements

First, and most of all, I would like to thank Assoc. Prof. Hakan Usta, for his expertise, assistance, guidance, and patience throughout the process of writing this thesis. Prof. Usta's assiduousness, deep knowledge, and enthusiasm for science has such an intense impact on me and my career. Without your help this work would not have been possible.

I would like to thank my jury members, Assoc. Prof. Evren MUTLUGÜN and Assoc. Prof. M. Serdar ÖNSES for their support and suggestions.

I am also appreciated to my lab-mate and senior Resul Özdemir for his endless help and gentleness during my research. And also I am appreciated to my lab-mates Hüsniye Ardıç Alidağ, Mehmet Özdemir and Ayse Can for their help during my research.

I would like to acknowledge that this study was supported by Research Fund of Abdullah Gül University (AGU-BAP), Project No: FYL-2018-115.

Last of all, I would like to thank my family with all my sincerity; my precious parents Nuh Mehmet and Rezan. I am also thankful to my wife, Erinç for her love, infinite patience and supports for every step of my life.

Table of Contents

List of Figures

List of Tables

Chapter 1

Introduction

1.1 Research History

It is widely recognized that energy and technology are essential pillars of contemporary civilization. Materials science and engineering, as one of the key interdisciplinary fields, set the ground for discovery of novel materials and techniques that are vital for the development of society. Based on the functional properties, these materials could be classified as structural and functional materials. The key characteristic of structural materials is the mechanical property. Structural materials are widely used in construction, packaging, transportation, industrial and sub-industrial production. On the other hand, functional materials have physical and chemical features, including optical, electrical, and magnetic properties. They are mainly used in advanced technologies including microelectronics, biology, and medicine. Furthermore, all materials are classified into two categories, namely organic and inorganic materials. In inorganic materials, the interaction between atoms is basically chemical bonds that could be of ionic, covalent, and metallic origin. Inorganic materials are highly stable in terms of their electronic properties. Traditional inorganic materials, especially silicon-based semiconductors, have been the key components of today's information technology, such as computers, cell phones, and flat panel displays. In the past two decades, inorganic nanomaterials, including zero-dimensional quantum dots, nanowires, nanotubes, have displayed remarkable progress. Due to the superior physical and chemical characteristics of nanomaterials, a wide range of interdisciplinary interests have emerged in the fields of physics, chemistry, biology, medicine, and engineering.[1]

Organic materials are less stable in terms of electronic properties compared to their inorganic counterparts because of the existence of van der Waals interactions between organic molecules. However, organic materials have unique properties over the inorganic materials; light-weight, low-cost, and compatibility with plastic substrates.[2] Some of the properties of organic materials such as being flexible, bendable and solution-processable can reduce the cost of fabrication via roll-to-roll processing and printing.[3]

Figure 1.1.1 Examples of organic semiconductor device applications.

In general organic materials are thought to be insulating materials due to their non-conducting properties. In the 1970s, Heeger et al. serendipitously discovered that polyacetylene can be highly conductive under certain doping conditions, and this conductivity is comparable to some inorganic conductors.[4,5] The great discovery of polyacetylene conductivity opens a new era for organic-based materials in electronic applications. In the 1980s and 1990s, numerous organic optoelectronic devices such as organic light-emitting diodes (OLED)[6], organic photovoltaics (OPV)[7], and organic field-effect transistors (OFET)[8] etc. have been developed.

1.2 Organic Field-Effect Transistors

Field effect transistors (FETs) are one of the most significant and fundamental constituents of electronic devices. Field effect transistors (FETs) have been largely used in current technologies such as information, communications, and computers. Conventional inorganic-based electronic devices, including inorganic single-crystal FETs and metal-oxide- semiconductor field-effect transistors (MOSFETs) are basically produced by using group 3 and 5 elements in the periodic table such as Si, Ge, and

GaAs. Inorganic semiconductors have become the major player of the industry due to their intrinsic properties such as good semiconductivity and high mechanical strength. Nevertheless, the fabrication process of inorganic transistors generally requires high temperature (>1000 °C). This prevents them being used with heat-sensitive substrates such as glass or plastic.[9,10] Hydrogenated amorphous silicon (α-Si:H) have been used as an active layer in TFTs and in LCDs due to its low temperature processibility. Inorganic materials have also not been preferred to be used in flexible and transparent displays because of being mechanically rigid. Thin film transistor (TFTs), a member of field effect transistor (FETs) family, has been used as an active matrix in electronic devices. TFT is composed of three types of materials, which are electrode, semiconductor, and dielectric.

1.2.1 Introduction of OFET

Until approximately 45 years ago, organic compounds had been considered as non-conductive. This consideration was confuted by the discovery of conductive polymers in the 1970s.[11–15] Today, a tremendous amount of research focuses on using these types of conductive organic materials in electronic applications. According to the level of resistivity, the conductive polymers can exhibit semiconducting or conducting behaviours depending on the doping levels.

An organic semiconductor is generally described as an organic material that has semiconducting features. Organic semiconducting materials could be small molecule, oligomer, or polymer-based materials depending on their distinctive properties and advantages over each other in different optoelectronic applications.

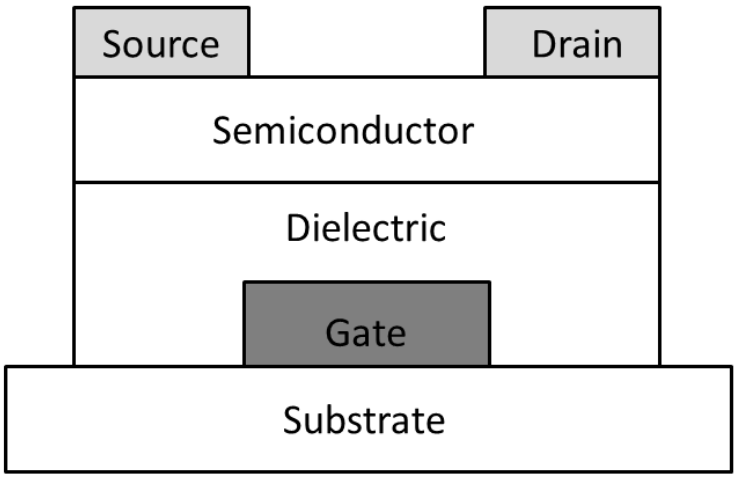

Figure 1.2.1.1 A basic OFET structure, in bottom-gate and top-contact device configuration.

Transistors that rely on organic semiconductors as an active layer to manage the flow of current are generally referred as OTFTs. The basic OFET structure is given in Figure 1.2.1.1. In a general sense, a field effect transistor (FET) consists of three fundamental parts: a semiconductor layer, a dielectric layer and gate/source/drain electrodes. The charge carrier movement direction in the semiconductor layer is parallel to the substrate surface from source to drain. The relationship between source, drain and gate electrode is that the gate controls the charge carrier density in the channel. When there is no gate bias voltage, there is no charge carrier transport through the channel, and no flow is monitored between source and drain electrodes. We can induce charge carriers in the semiconducting layer by applying voltage on the gate electrode, which causes polarization in the dielectric layer. OFET applications could be classified according to the type of charge carriers; these are *p*-channel in which charge transporting is made by holes and *n*-channel in which charge carriers are electrons.

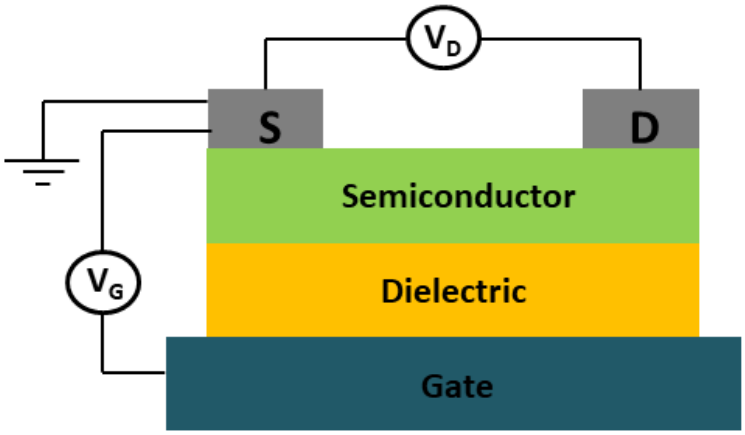

Figure 1.2.1.2 Schematic diagram of an OFET device structure.

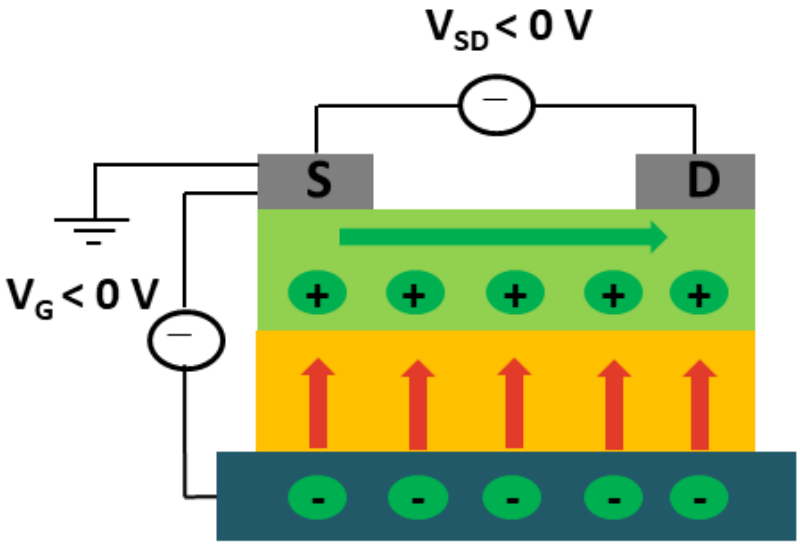

Figure 1.2.1.3 Schematic diagram of *p*-channel OFET.

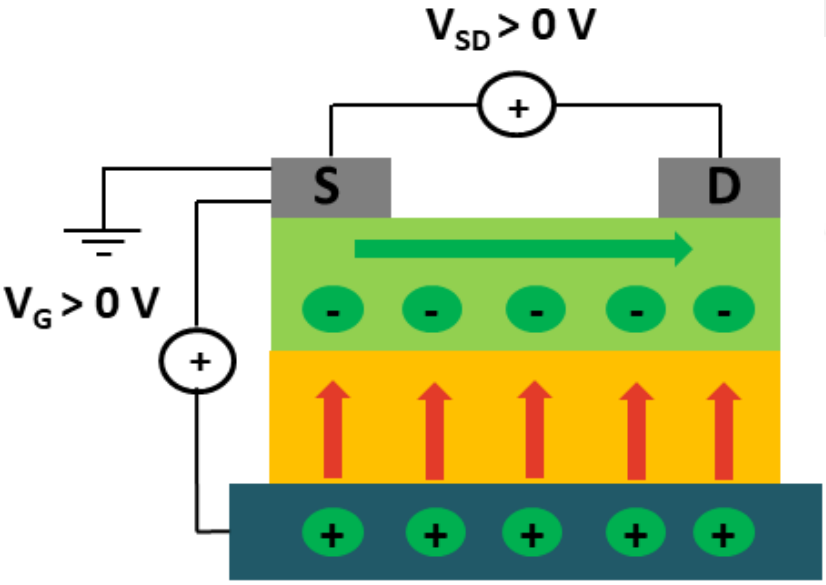

Figure 1.2.1.4 Schematic diagram of *n*-channel OFET.

Organic field effect transistors mostly require two electrical characterizations: **(i)** to evaluate transfer characteristics, apply constant drain–source voltage (V_{SD}), scan gate voltage (V_G) and measure the drain–source current (I_{DS}) (Fig. 1.2.1.4); **(ii)** to obtain output characteristics, apply constant gate voltage (V_{GS}), scan drain–source voltage (V_{DS}) and measure drain–source current (I_{DS}). Charge carrier mobility (μ), threshold voltage (V_T) which are extracted from the saturation region by using this equation:

$$\mu_{sat}=(2\ I_{DS}L)/[WC_i(V_G- V_T)^2]$$

and current on/off ratio (I_{ON}/I_{OFF}) is the key parameter to measure the performance of an organic field effect transistor.

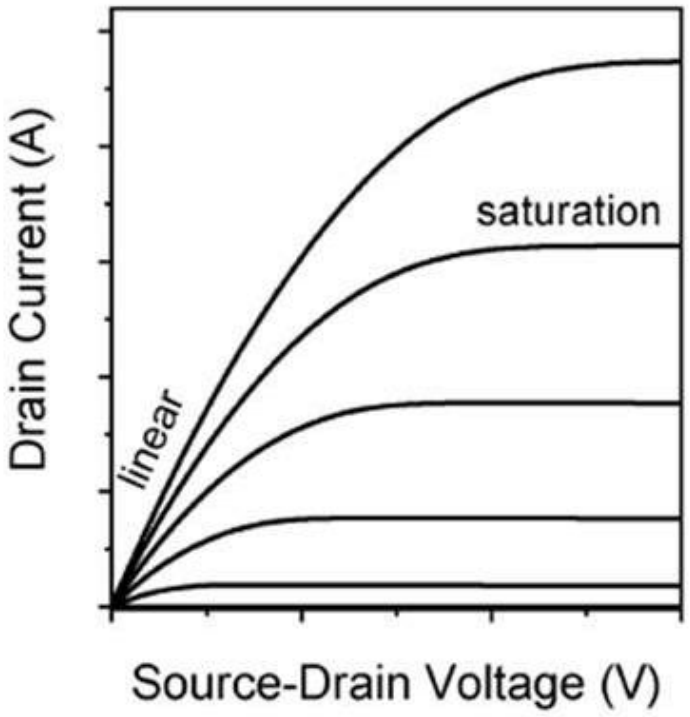

Figure 1.2.1.5 Typical OFET output curve.

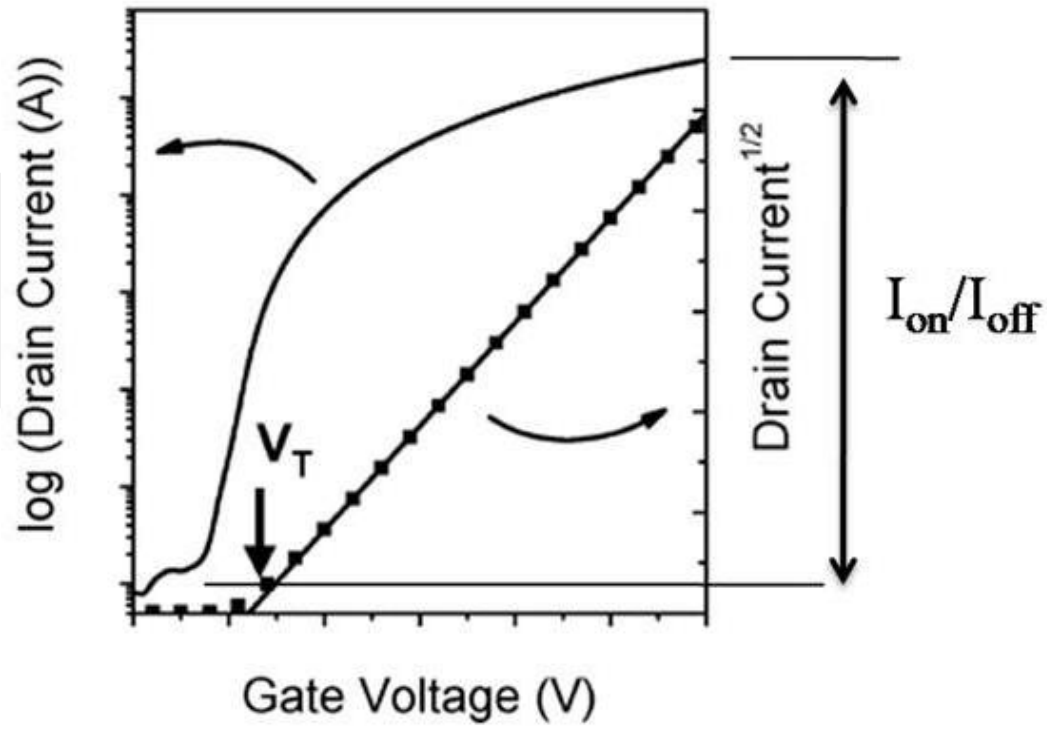

Figure 1.2.1.6 Typical OFET transfer curve.

The varied deposition orders of the device layers results in different device architectures for OFET. There are four possible device structures depending on the gate electrode position and the contact between the drain/source electrode and the semiconductor: bottom gate/top contact (BG/TC), bottom gate/bottom contact (BG/BC), top gate/top contact (TG/TC) and top gate/bottom contact (TG/BC).[13,16] Although device performance is primarily governed by semiconductors, device architecture can greatly affect charge injection and contact resistance. For p-type materials, BG/TC and BG/BC structures are often used, while TG/BC structures are mainly used for ambipolar and n-type OFETs to reduce the effects of oxygen and water. BG/BC and TG/BC structures are generally considered to have a smaller injection barrier due to different device injection pathways.[17,18]

1.2.2 Types of Organic Semiconductors

Polymer-based and small molecule-based organic semiconducting materials are widely used in organic electronic devices. These materials will be briefly explained in the following subchapters.

1.2.2.1 Polymers

Polymers are high molecular weight organic structures formed by linking a large number of repeating units. There are two types of polymers, natural and synthetic. Examples for natural polymers are rubber, protein, wool, hair, and nails. In living organisms, carbohydrates, deoxyribonucleic acid (DNA) and ribonucleic acid (RNA), which are also polymeric, are called biopolymers. Synthetic polymers are commercially produced and have a wide range of properties and applications. Polymer chains are formed by chemical reactions that allow a large number of units to bond sequentially through covalent bonds. The polymers are separated into two groups as conjugated and non-conjugated polymers according to their structure and the nature of their chemical

bonds between the monomeric units. Although both conjugated and non-conjugated polymers exhibit similar mechanical properties, their electrical properties could be totally different. Polymers were initially considered as good insulators and used as a photoresist material in the semiconductor industry. In 1977, halogen-doped polyacetylene having relatively a high conductivity opened a new era for polymers.[19] The doped polyacetylene exhibits a conductivity of 10^5 Sm^{-1}. However, it is very vulnerable to oxygen, and this polymer is not soluble in common organic solvents. For non-conjugated polymers, the bond between each of the hydrogen atom and carbon atom is formed by overlapping of hydrogen 1s orbitals and carbon sp^3 hybridized orbitals. In this type of bonding architecture, a large amount of energy is required for electrons to move from one orbital to another. In other words, the energy band gap between the filled and empty orbitals of non-conjugated polymers is very high. This structural property results in non-conjugated polymers acting as insulating material. On the other hand, the chemical bond structure of the conjugated polymers is based on the structure of the backbone formed by single and double bonds. In conjugated polymers, some of the chemical bonds are formed by sp^2 orbitals of carbon atoms and 1s orbitals of hydrogen atoms. Other parts of chemical bonding are formed by carbon atoms with p orbitals.[20] There are π bonds between these carbon atoms. Because of this, less energy is required to transport an electron from a π orbital to a π^* orbital, the energy gap between filled and empty bands is relatively small compared to non-conjugated polymers.[21] In conjugated polymers alternation of single and double bonds lead to electron delocalization. Delocalized electrons create a band structure that exhibits semiconducting or metallic properties. Besides, these electrons act as charge carriers and move along the polymer chain.[22]

There are two figures of merit for conjugated systems. The first one is the existence of "conjugated double bonds" through the backbone. The second one is mobility; charge carriers (electrons and holes) must move through the molecular structures to enhance conductivity.[23]

Conjugated double bond comprises a σ-bond and a π-bond. σ-bond is a very strong covalent bond, whereas π-bond is a relatively weak bond. Normally π-bond electrons tend to be localized, but in conjugated systems thanks to overlapping between neighboring π-bonds electrons are highly delocalized. Therefore, charge carrier transport happens by the help of continuous overlapping of π-orbitals.[24]

The alternation of single and double bonds in conjugated systems causes energy gap to reduce. The highest occupied molecular orbital (HOMO) is equivalent to valence band, and the lowest unoccupied molecular orbital (LUMO) is equivalent to the conduction band of inorganic semiconductors. The band gap energy between HOMO and LUMO levels is related to the degree of π-conjugation.

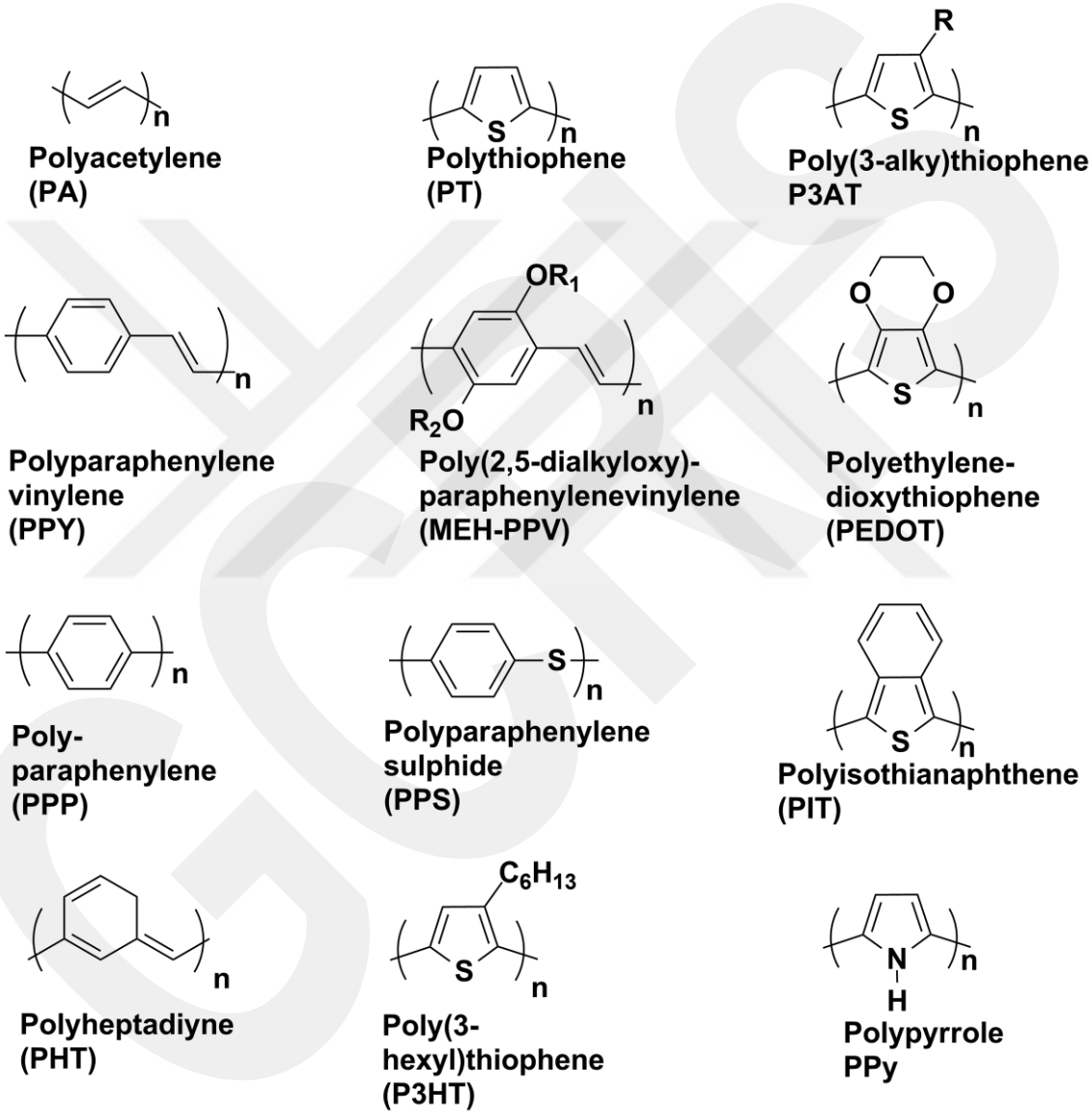

Figure 1.2.2.1.1 Chemical structures of some conjugated polymers.

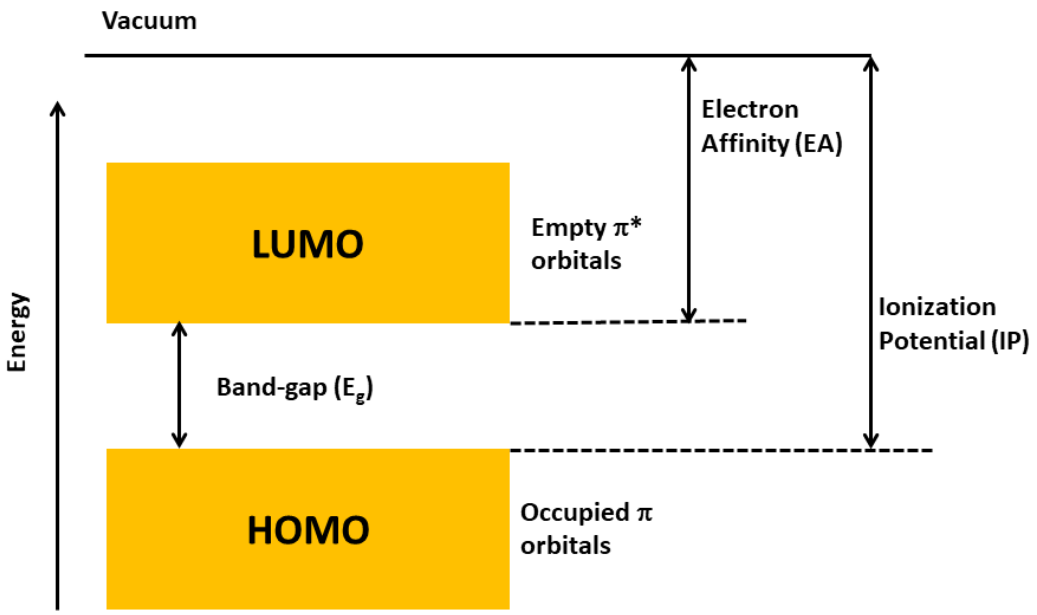

Figure 1.2.2.1.2 Organic semiconductors energy band diagram.

Organic materials are considered as insulators due to their initial neutral state and wide band gap energy. To solve this problem, oxidation and reduction reactions are used to succeed *p*-channel (hole conduction) and *n*-channel (electron conduction) operations. These charge carriers pass through the conjugate backbone in the electric field. Most of the organic-based materials in the literature are *p*-channel polymers.

The conjugated organic system can be used as a semiconductor due to strong π-π overlap. When additional charge is added to the system, the charge will delocalize throughout the molecule/polymer.

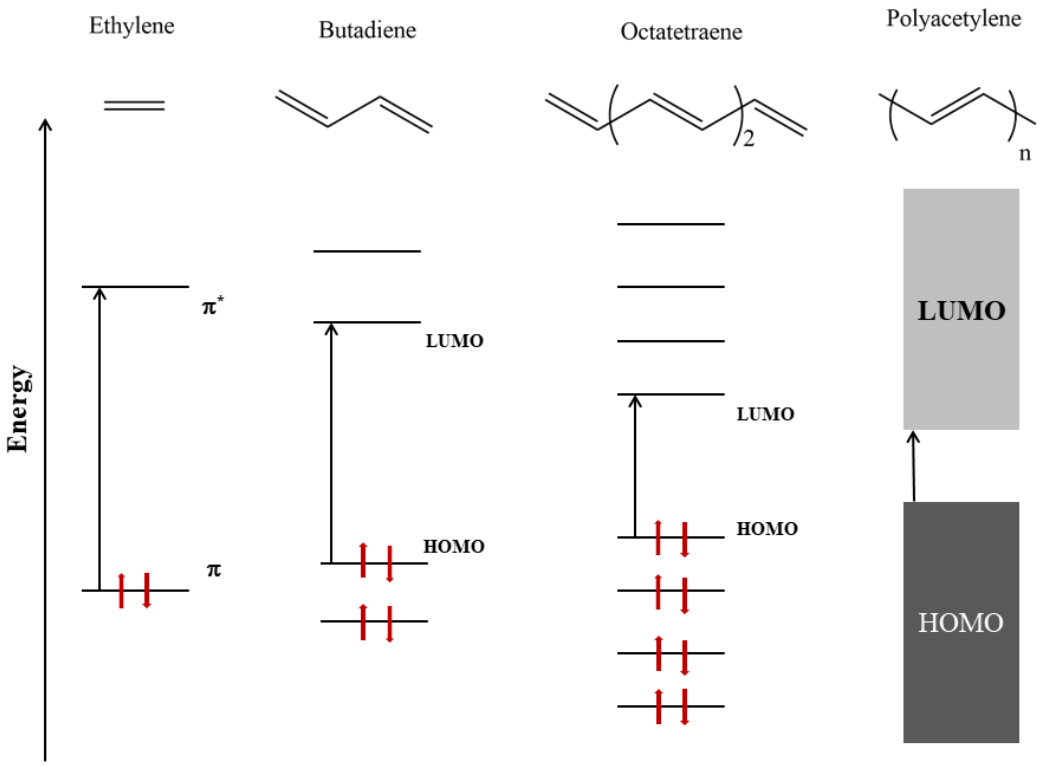

Figure 1.2.2.1.3 The **e**ffect of conjugation length on band gap energy.

1.2.2.1 Small molecules

Small molecular semiconductors are low molecular weight organic compounds containing aromatic hydrocarbons. These semiconductors could usually be grown on a desired substrate by a thermal evaporation method in a vacuum system. On the other hand, conjugated polymers can be dissolved in suitable solvents and can be deposited by spin-coating or ink-jet printing. The ability of small molecules to be coated on intended substrate at desired thickness by evaporation allows obtaining more complex multi-layer structures compared to polymers. There are several advantages of using π-conjugated small molecular systems instead of polymers, which are enhanced solubility, higher crystallinity, better synthetic reproducibility, and higher degree of purity.[25–28] The electrical and optical properties of organic semiconductors can be easily adjusted by synthesizing different sizes of molecules and adding functional groups into organic structures.[22] Pentacene, tetracene and rubrene are among the widely studied organic small molecules containing a polycyclic aromatic structure. Pentacene and copper phthalocyanine (CuPc), which have relatively high charge-carrier mobilities, have extensively been used as active layers in OFETs and solar cells.[29]

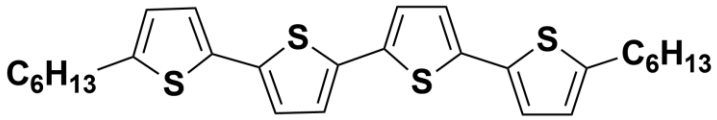

DH_4T

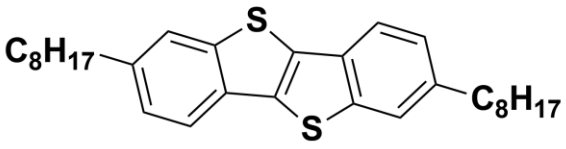

C8-BTBT

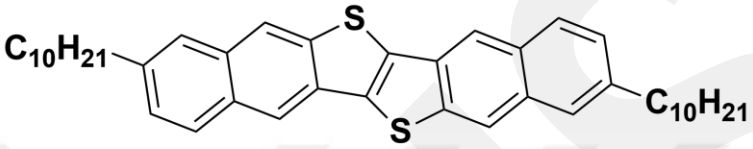

C_{10}-DNTT

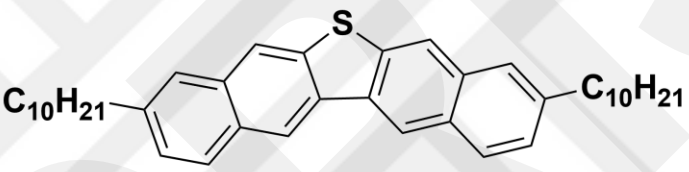

C_{10}-DNT-VW

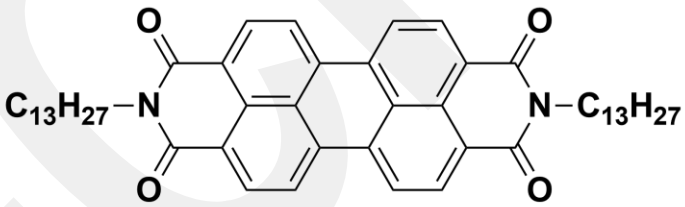

PTCDI-C_{13}

Figure 1.2.2.2.1 Chemical structures of some conjugated small molecules.

1.2.2.2.1 Pentacene

One of the main difficulties in increasing the performance of OFETs is the development of conjugated semiconductors with good mobility and good stability in ambient conditions.[30] Pentacene is one of the highly used acenes in OFET devices because of its high charge-carrier mobilities of up to 1 cm^2/Vs. [31,32] The chemical formula of pentacene is $C_{22}H_{14}$, and it has a molecular weight of 278.36 g/mol. As shown in Figure 1.2.2.2.1.1, it is a polycyclic aromatic hydrocarbon consisting of five fused benzene rings. The benzene rings are fused in a linear fashion to form a planar molecular structure through which delocalized electrons could freely move.

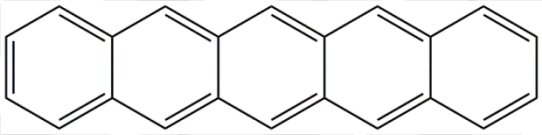

Figure 1.2.2.2.1.1 Chemical structure of pentacene.

1.2.2.2.2 Indenofluorene

Indenofluorene, which contains indene and fluorene groups, is also a conjugated polycyclic hydrocarbon. Indene, which has the chemical formula of C_9H_8, is a flammable polycyclic hydrocarbon. It consists of a cyclopentene ring fused with a benzene ring. Indene is not soluble in water, but soluble in several organic solvents. The liquid form of indene is colorless, but it is usually pale yellow in the solid-state. Fluorene is also a member of polycyclic aromatic hydrocarbon.[33] It forms white crystals and displays a characteristic odor similar to naphthalene. According to the indene and fluorine attachment points, five regioisomers could be formed, each with its own properties, applications, and research areas.[34]

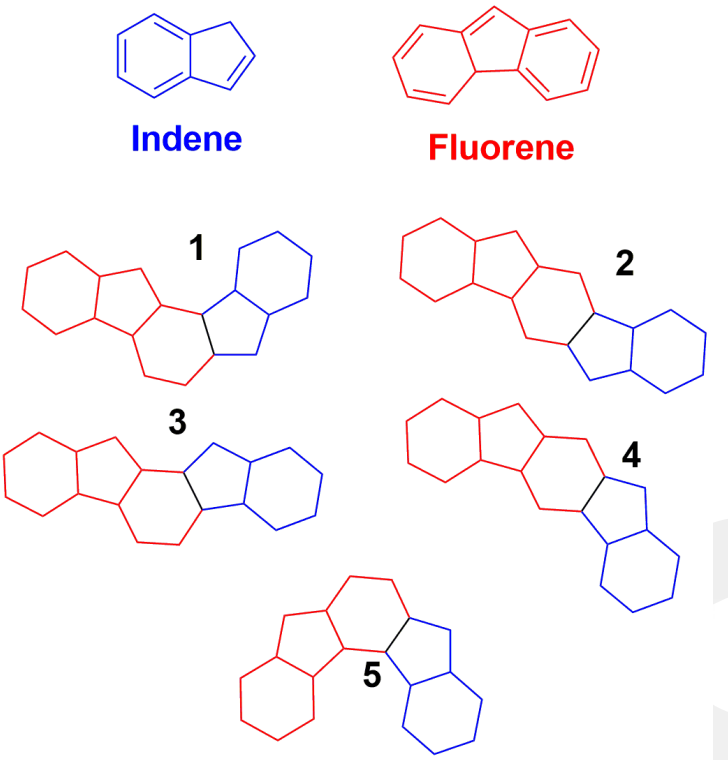

Figure 1.2.2.2.2.1 Chemical structures of Indenofluorene regioisomers.

The indenefluorene family consists of five structural isomers that are difficult to distinguish into multiple naming and numbering strategies. There are indeno[1,2-a]fluorene (1), indeno[1,2-b]fluorene (2), indeno[2,1-a]fluorene (3), indeno[2,1-b]fluorene(4), indeno[2,1-c]fluorene (5). Note that indeno[1,2-b]fluorene is the most commonly used regioisomer in organic electronic applications.[33]

1.2.3 Dielectric Materials

Dielectric materials play an important role in OFETs. In a typical field-effect transistor, dielectric film is used to isolate gate electrode from organic semiconductor, and it is in direct contact with the semiconductor layer. Historically, silicon dioxide (SiO_2) has dominated electronic industry because of its excellent compatibility with the silicon substrates.[35] However, there is a strong need for new insulating materials because next-generation transistors need to be fabricated on substrates other than silicon.[36] It is found disadvantageous that the processing of Si substrates and dielectrics requires costly processing methods and lithographic techniques.[37] The production of thermally oxidized SiO_2 requires high temperature. This process causes high energy consumption making it impossible to grow on flexible substrates. On the other hand, the capacitance density is small due to the low dielectric constant of SiO_2, which causes OFETs to have high operating voltages of more than 30 V. This could be a problem for applications requiring low operating voltage such as RF-ID tags, portable sensors, electronic papers, and mobile devices. For OFETs, the new dielectric material must have a high dielectric constant, low leakage current, high thermal stability, and high breakdown voltage.[38] High capacitance in OFETs allows the transistors to have low operating voltage and high mobility.[39] At the same time, maintaining a low leakage current reduces power consumption in the device. Insulating materials with high dielectric constant reduce the transistor operating voltage in integrated circuits for high current conduction. In addition to having a high dielectric constant, dielectric materials could be dissolved in organic solvents and then coated on any surface (fabrics, plastic, glass, etc.) by using simple solution-based techniques. Therefore, it is important from technical and financial points of view to easily process dielectric materials to commercialize in electronics industry. Prior to organic semiconductor deposition, functionalization of the dielectric surface is crucial to achieve high device performance. Dielectric surface conditions have great impact on electrical properties of OFET devices.[40]

1.2.3.1 Inorganic Dielectrics Materials

The most commonly used gate insulator in OFET technology is SiO_2 with a dielectric constant of 3.9.[41] The reason behind the silicon's high popularity is the advancements in fabrication technologies. With its high quality and smooth surface, silicon dioxide could be obtained directly on silicon via thermal oxidation method and could provide reproducible results for various transistor applications.[27] However, SiO_2 has reached its limits as a dielectric material. The disadvantage of SiO_2 is that electrons between the semiconductor and the insulating layer are trapped by hydroxyl groups called "silanols".[42] Reducing thickness of the SiO_2 insulator layer to increase its capacitance could be one possible solution to overcome the disadvantages of SiO_2. However, this leads to increased leakage current and high power consumption, which reduces the reliability of the device. When 1 V is applied to a capacitor with a thickness of 3 nm SiO_2, the leakage current is 10^{-5} A/cm^2. When the thickness is reduced to 2 nm, the leakage current value significantly increases to 10 A/cm^2.[27] For this reason, gate dielectrics with high dielectric constant are used to minimize leakage current. In this context, along with the reaching of device limits of SiO_2, many researchers are carrying out research on alternative inorganic gate insulating materials such as hafnium dioxide (HfO_2), tantalum pentoxide (Ta_2O_5), aluminium oxide (Al_2O_3), yttrium oxide (Y_2O_3) and titanium dioxide. However, high annealing temperatures of these materials make it difficult to grow on plastic substrates.[43] In addition, costly processing techniques increase costs in electronic technology. At the same time, hydroxyl (-OH) groups are generally present in metal oxides with this high dielectric constant, and these hydroxyl groups cause unwanted interfacial environment between the semiconductor and the insulator. These issues adversely affect the device's parameters such as charge-carrier mobility, stability, and leakage current.

1.2.3.2 Organic Dielectrics Materials

The search for alternative dielectric materials to avoid undesirable properties of silicon dioxide is a rational step for realizing high-performance OFETs. To this end, polymers could be used as a dielectric layer. The polymers have simple processing steps, good mechanical properties, and a relatively low dielectric constant. Increasing the polymer thickness to reduce leakage current at the dielectric-semiconductor interface causes high operating voltages due to their low dielectric constants.[44] In addition, insulating polymers could be used in top and bottom gate device geometries because they do not damage the semiconductor morphology.[45] However, small protrusions or pits on the polymer insulating surface could negatively affect the device field-effect mobility.[43]

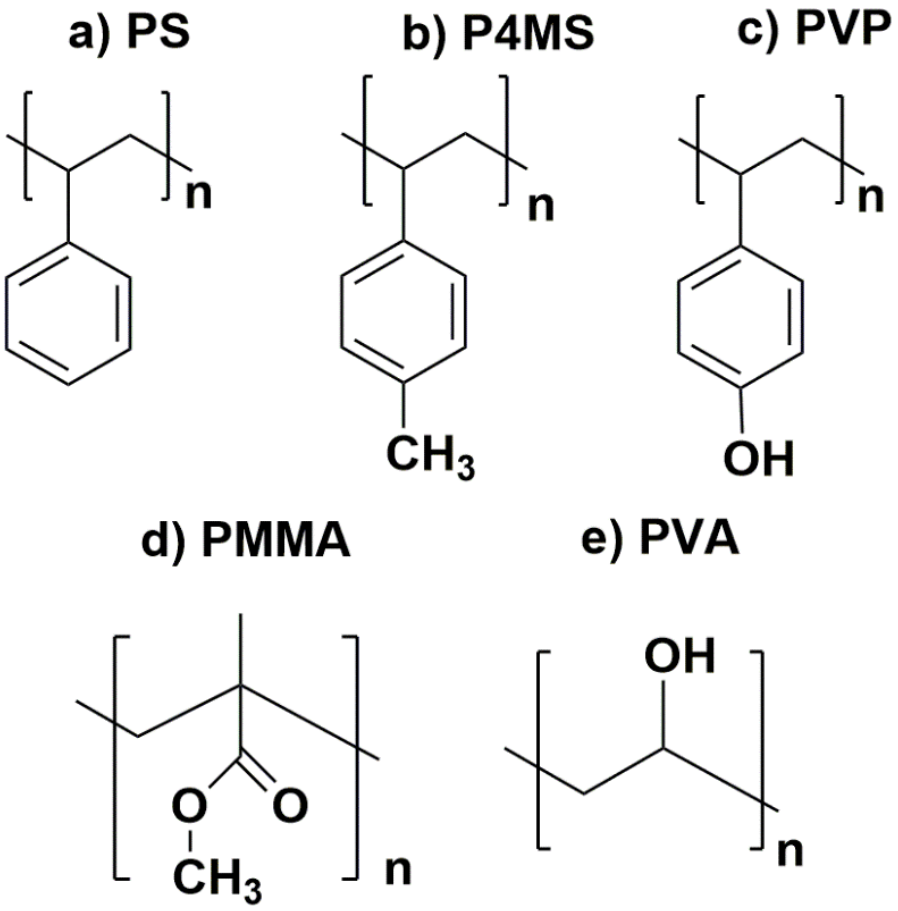

Figure 1.2.3.2.1 Chemical structures of polymer dielectric materials.

1.3 Microstructure and Molecular Alignment

The organic semiconductor thin-film includes a mixture of polycrystalline and amorphous phases, and charge transfer mechanism does not work well between these two regions due to their different abilities of charge transportation. Therefore, proper solid-state arrangement is critical to achieve efficient charge transport, and this is achieved by performing proper molecular engineering on organic materials.

Characterization of organic thin-film could be carried out by X-ray diffraction (XRD) and atomic force microscopy (AFM) techniques. Molecular parameters such as π-π stacking distances, *d*-spacings, and morphologies could be obtained by using these techniques.

In addition, the arrangement of small molecules or polymer chains has a significant impact on transistor device performance. Poly(3-hexylthiophene) exhibits two different types of orientations based on processing conditions and dielectric surface properties.[46] In the edge-on orientation, π-π stackings are parallel to the direction of charge carrier movement. However, in face-on orientation, π-π stacking alignment is perpendicular to the direction of charge carrier movement. By changing the molecular orientation from face-on to edge-on, mobility has dramatically decreased by more than two orders of magnitude.

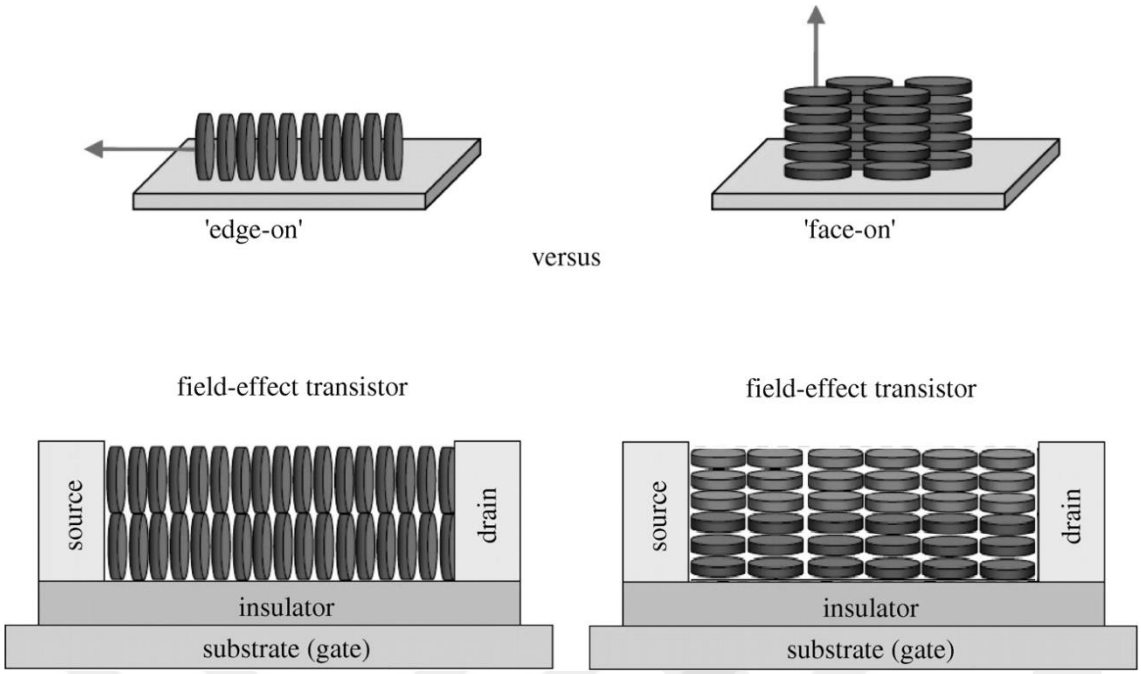

Figure 1.3.1 Edge-on and face-on orientations of ordered P3HT domains relative to the transistor substrate.

Dielectric surface modification is one of the most important steps in the fabrication process of OFET devices. Functionalization of the dielectric surface is critical to achieve high device performance prior to organic semiconductor deposition. Dielectric surface environments have a large impact on the electrical performance of OFET devices.

Figure 1.3.2 summarizes the changes in mobility of various semiconductors over the course of time. In the first OFET study, the mobility of OFET with the active layer of polythiophene was found to be about 10^{-5} cm^2/Vs.[46] The performance of OFETs has constantly increased after this work. In general, the mobility of polythiophene has increased about 10^5 times. The performances of some OFETs have now come to the point where they can compete with the preferred amorphous silicon FETs. The field-effect mobility of OFETs utilizing active layer of pentacene has reached to the level of amorphous silicon (α-Si:H).[47–51] The increasing mobility of organic semiconductors which is comparable with the α-Si:H mobility is the indicative of the prospect of forming screens on flexible plastic substrates in the electronic technology.

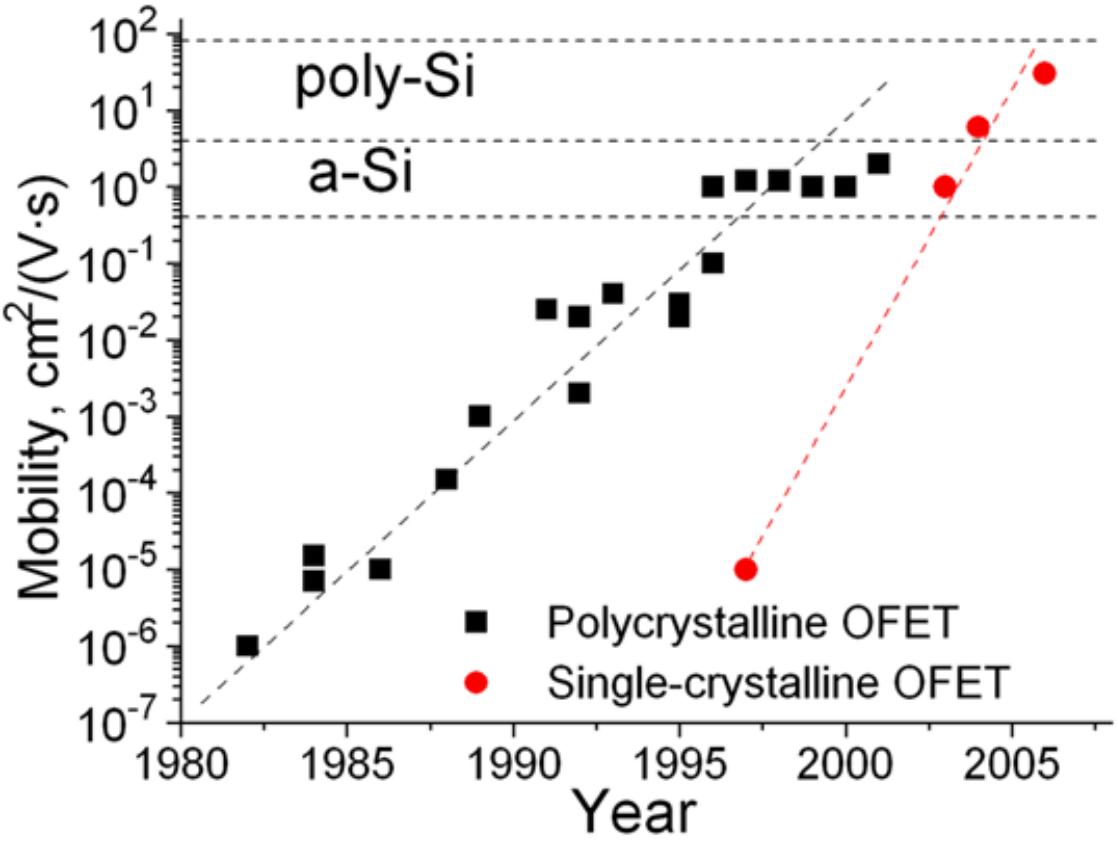

Figure 1.3.2 Progress in the performance of organic semiconductor.[22]

1.4 Research Strategy and Overview of This Thesis

N-type organic semiconductors constitute an important class of semiconductor materials and have recently attracted a wide range of scientific and technical interest to achieve low cost, mechanically flexible, large area and printed optoelectronic devices such as organic field effect transistors (OFETs) and organic photovoltaics (OPVs). So far, air-stable and solution-processable *n*-type semiconductors have mainly reported on donor-acceptor-donor (D-A-D) type π-conjugated systems. Their charge carrier mobility exceeds that of amorphous silicon (μ_e > 0.5 cm^2/Vs) and have been implemented in polymeric organic field effect transistors (OFETs).

Nevertheless, very few solution-processable *n*-type small molecular π conjugated systems are known to operate in ambient. This is mainly due to the difficulty of achieving such low HOMO-LUMO energy gaps (<2.0 eV) and sufficiently low LUMOs (<-4.0 eV) within a limited molecular π-conjugation length. To date, although many *p*-channel molecular semiconductors with high mobility (>40 cm^2/Vs) have been developed with good solution-processibility and ambient stability, there are very few *n*-channel small molecules exhibiting these characteristics. Therefore, the continued efforts to design and develop *n*-channel small molecules are crucial to fully reveal their technological potentials and to study the fundamentals of electron charge transport processes in molecular solids.

In chapter two, our efforts on designing, synthesizing and characterizing of two new ladder-type solution-processable and air-stable *n*-type small molecules, **TIPS-IFDK** and **TIPS-IFDM** are described. Fabrication and performance analysis of these novel organic semiconductors are reported.

Among the molecular semiconductors studied to date, small molecules with electron-deficient π-architectures and low LUMO energy levels constitute an important class of materials for air-stable electron transport in p-n junctions, bipolar transistors,

and organic complementary-like circuitry (CMOS). In addition, π-deficient small molecules can function as non-fullerene electron acceptors for use in bulk-heterojunction organic solar cells. However, among the molecular semiconductors developed to date, air-stable and solution-processable *n*-channel molecular semiconductors are still scarce. Therefore, the continued research efforts to this end are very important to enhance structural variety and device performances of these types of organic semiconductors, and to better understand their structure-property-device relationships.

Chapter 2

Solution-Processable Rod-Shaped Triisopropylsilylethynyl Indenofluorenes: Synthesis, Single-Crystal Structures, Optoelectronic Properties, and N-Channel Organic Field-Effect Transistor Applications

2.1 Introduction

Solution-processable polycyclic aromatic hydrocarbons (PAHs) with good electron-accepting and transporting properties are very attractive semiconducting materials for n-channel organic field-effect transistors (OFETs), complementary circuits, and photovoltaics. While solution processability is key to roll-to-roll fabrication of low-cost, flexible, and large area devices, structural versatility of the π-systems allows for the realization fine-tuned (opto)electronic properties. The functionalization of PAHs to impart solubility in common organic solvents and to induce electron-accepting/transporting properties could be achieved via exploratory synthesis, which has been widely exploited for the development of novel small/macro-molecular structures with unprecedented properties. Rational incorporation of strongly electron-withdrawing substituents such as –CN, -F, and $-C_nF_{2n+1}$ have particularly been important for reducing frontier orbital energy levels of PAHs and facilitating electron-transport processes in (opto)electronics. For solution-processable PAH semiconductors, it's very critical to select properly sized π-skeleton to reach a delicate balance between solubility and minimum effective charge carrier π-delocalization. To this end, relatively

small-sized indenofluorene (IF) has recently become an attractive π-core as a functionalizable coplanar, ladder-type aromatic PAH.[49,52] Although IF derivatives have been widely explored for over seventy years in organic literature,[53] its potential as a functional charge-transporting material has recently been revealed. In 2008, Usta et al. has pioneered the early studies demonstrating carbonyl (C=O) and dicyanovinylene ($C=C(CN)_2$) functionalizations on indenofluorene five-membered rings could lead to a novel class of high performance, ambient-stable n-channel semiconductors in OFETs. These compounds are named "indenofluorenediketone (IFDK)" and "indenofluorenedimalononitrile (IFDM)", and they exhibit highly stabilized LUMO energies (-3.5 eV - -4.2 eV), good reversible reductions, photo/thermal stabilities, and solution processabilities. Later, following this original study, numerous IFDK and IFDM derivatives have been synthesized yielding electron mobilities as high as 1.0 cm^2/Vs.[54] It is noteworthy that non-functionalized indenofluorene π-structures display only p-channel characteristics due to the fact that their LUMOs are energetically too high (> -3.0 eV) and the HOMOs (-5.2 eV) align well with air-stable conductive electrodes (e.g. Au: 5.1 eV).[34,55] Specifically, the detailed studies on indenofluorene-based semiconductor libraries by fine-tuning frontier orbital energies have led to the finding of LUMO threshold value (-4.0 - -4.1 eV) for ambient-stability. Considering that there are still very few solution-processable and low-LUMO n-type semiconductors in the literature, continued design and synthesis of novel molecular architectures are important. Especially, small molecules that could be synthesized in few steps (three or less) are very valuable for future technological implementation of these materials in low-cost optoelectronics. On the other hand, maintaining a large HOMO-LUMO energy gap while stabilizing LUMO energy level is crucial for (opto)electronic devices to prevent undesired hole injection/transport characteristics through HOMOs.

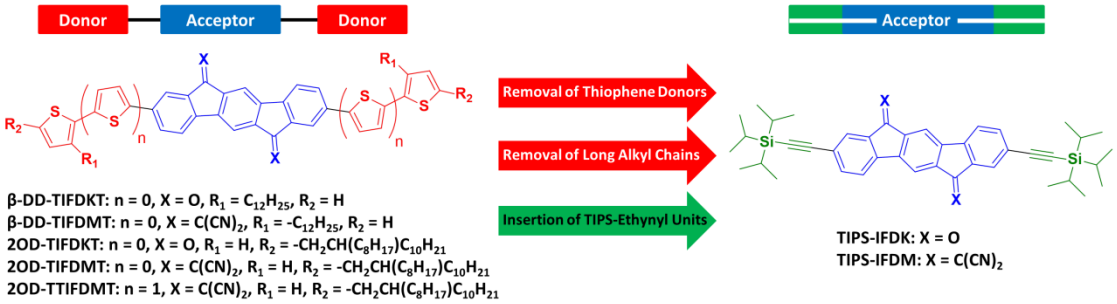

Figure 2.1.1 The chemical structures of newly designed **TIPS-IFDK** and **TIPS-IFDM** compounds as compared to previously reported representative electron-transporting indenofluorene derivatives.

Herein, completely different than the earlier reports on solution-processed electron-transporting indenofluorenes, in which alkyl or β-/α,ω-alkyl substituted donor-units are placed at molecular termini, we envision to completely remove donor end-units and long linear/swallow-tailed liphophilic alkyl substituents, and to introduce shape-persistent, rod-like (trialkylsilyl)ethynyl (R_3Si-C≡C-) groups (Figure 2.1.1). The presence of trialkylsilyl group significantly enhances the solubility of insoluble PAHs and increase their photochemical/ambient stability, which has opened new venues for the realization of solution-processed (opto)electronic devices.[47–49,56–58] In addition, the nature of the alkyl substituents in (trialkylsilyl)ethynyl groups has been discovered to drastically alter the semiconductor solid-state packing motifs, and, thus, the corresponding charge-carrier mobilities in OFETs. Following this strategy, numerous solution-processable molecular semiconductors, most of which comprise formerly insoluble acene π-frameworks, have been prepared and characterized in OFETs in the past decade.[59,60] It is noteworthy that silicon is one of the few elements that has a lower electronegativity than carbon and can still form a strong covalent bond with carbon. This imparts a great electron density, thus polarizability, on the short, branched alkyl groups of trialkylsilyl ($-SiR_3$) substituents, which allows the formation of strong attractive London-dispersion forces with the organic solvents. Alkyne linkages are employed between sterically-bulky triisopropyl substituents and the central indenofluorene cores as a spacer to result in π-stacked (vide infra) shape-persistent, rod-like structures with practically no conformer formation. Due to its quasi-cylindrical electronic symmetry, alkyne linkages are key to accommodate steric/conformational constraints and the presence of sp-hybridized carbons should stabilize frontier orbital energies of the new molecules to assist its electron-accepting properties. In the current

molecules, π-frameworks are synthesized with R_3Si-C≡C- groups along the long molecular axis, which is very different than most of the previously reported semiconductors that are typically substituted with R_3Si-C≡C- groups along the short molecular axis. To the best of our knowledge, this is the first time that a molecular semiconductor substituted with (trialkylsilyl)ethynyl groups along the long molecular axis is characterized in OFETs. Note that although there has been few recent studies reporting pentacene derivatives substituted with (trialkylsilyl)ethynyl at X,Y-positions (long molecular axis), these studies did not demonstrate any OFET device fabrication and characterization.[61–63] Therefore, the present molecules would constitute a valuable platform to understand whether (trialkylsilyl)ethynyl functionalization along long molecular axis is a practical strategy to realize π-stacked solid-state packing and solution-processed OFETs with good electron mobilities.

2.2 Experimental

2.2.1 Materials and Methods

Unless otherwise noted, all reagents were purchased from commercial suppliers and used without as received. All non-aqueous reactions were carried out in dried glassware under an inert atmosphere of N_2. Column chromatography was carried out with 230-400 mesh silica gel under the effect of gravitational force with or without additional air pressure. Thin-layer chromatographies (TLC) to monitor reaction progresses and chromatographic fractions were performed on alumina sheets covered with silica gel 60 F254. Melting points were determined on a Electrothermal IA9000 series digital melting point apparatus. Proton and carbon nuclear magnetic resonance (^1H and ^{13}C NMR) spectra were recorded in deuterated chloroform ($CDCl_3$) using a Bruker 400 spectrometer (^1H at 400 MHz and ^{13}C at 100 MHz). Elemental analyses were recorded on a LecoTruspec Micro model instrument. Thermal characterizations of thermogravimmetric analysis (TGA) and differential scanning calorimetry (DSC) were performed under nitrogen at a heating rate of 10 °C/min using Perkin Elmer Diamond model instruments. Cyclic voltammetry measurements were carried out using BAS-Epsilon potentiostat/galvanostat from Bioanalytical Systems Inc. (Lafayette, IN)

equipped with a C3-cell stand electrochemical station. High-resolution mass spectra were measured on a Bruker Microflex LT MALDI-TOF-MS instrument. UV-vis absorption spectra were recorded on a Shimadzu UV-1800 UV-Vis spectrophotometer. The optimization of the molecular geometries and total energy minimizations were obtained by Gaussian 09 program using density functional theory (DFT) with B3LYP method and 6-31G** basis set.

2.2.2 Synthesis and Characterization

Synthesis of reference semiconductor molecules **β-DD-TIFDKT** and **β-DD-TIFDKM** were performed in accordance with our previously procedures.[55]

2.2.2.1 Dimethyl 4,4''-dibromo-[1,1':4',1''-terphenyl]-2,2''-dicarboxylate (1)

Tetrakis(triphenylphosphine)palladium (0.529 g, 0.458 mmol), and sodium carbonate solution (1M) were added into a solution of 1,4-benzenediboronic acid bis(pinacol) ester (2.518 g, 7.63 mmol), methyl 5-bromo-2-iodobenzoate (5.697 g, 16.71 mmol), and aliquat 336 (0.911 mL, 1.98 mmol) in 55 mL of anhydrous toluene under nitrogen. The resulting mixture was stirred at 135 ℃ for 2 days. After completing reaction, it was allowed to cool down to room temperature. The reaction mixture was poured into water to yield a white precipitate. Then, it was extracted with hexane, dried with Na_2SO_4, filtered and concentrated to get the crude product. The crude was then purified through column chromatography on silica gel using dichloromethane as mobile phase to afford the final product as a white crystalline solid. (3.50 g, 91% yield).^{1}H NMR (400 MHz, $CDCl_3$), δ (ppm): 3.71 (s, 6H), 7.32 (m, 6H), 7.67 (dd, 2H, J = 8.0 Hz and J = 2.0 Hz), 8.00 (d, 2H, 2.0 Hz).

2.2.2.2 2,8-dibromoindeno[1,2-b]fluorene-6,12-dione (2)

The solution of dimethyl 4,4''-dibromo-[1,1':4',1''-terphenyl]-2,2''-dicarboxylate **(1)** (0.550 g, 1.09 mmol) in 76-78% H_2SO_4 (50 mL) was kept stirring overnight at 120 ℃. The reaction was then cooled down to room temperature and quenched with ice to yield a dark red precipitate. The precipitate was collected by vacuum filtration, and washed with water, saturated solution of sodium hydrogen carbonate, and methanol, respectively, to obtain the crude product. The crude was then purified through thermal gradient sublimation under high vacuum to afford pure product as a cherry red crystalline solid (0.427 g, 89% yield). During the sublimation single-crystals of this compound was also obtained. m.p.> 390 °C. Anal.calcd. for $C_{20}H_8O_2Br_2$: C, 54.58; H, 1.83 Found: C, 54.70; H, 1.96.

2.2.2.3 2,8-bis((triisopropylsilyl)ethynyl)indeno[1,2-b]fluorene-6,12-dione (TIPS-IFDK)

A mixture of 2,8 dibromoindeno[1,2-b]fluorene-6,12-dione **(2)** (0.500 g, 1.136 mmol), CuI (0.01 g, 0.057 mmol) and $Pd(PPh_3)_2Cl_2$ (0.079 mg, 0.113 mmol) were dissolved in dry Et_3N:DMF (20ml:40 mL), and stirred for 5 min. Afterward, (triisopropylsilyl)acetylene (0.497 g, 2.726 mmol) was added, and the resulting mixture was heated and stirred at 110°C under nitrogen for 18 h. After completing reaction, the reaction mixture was allowed to cool down to room temperature, and quenched with water. The reaction mixture was extracted with chloroform, dried with Na_2SO_4, filtered and concentrated to get the crude product as dark red oil. The crude was then purified through column chromatography on silica gel using $CHCl_3$:Hexane (2:1) as mobile phase to afford the final product as a pink neon solid. (0.467 g, 64% yield). ^{1}H NMR (400 MHz, $CDCl_3$), δ (ppm): 1.15 (s, 42H), 7.50 (d, *J*=8.0 Hz, 2H), 7.65 (dd, *J*=8.0 Hz, 2H), 7.78 (s, 2H), 7.81 (s, 2H); ^{13}C NMR (100 MHz, $CDCl_3$): δ (ppm): 11.26, 18.66, 93.80, 105.67, 116.37, 120.52, 125.04, 128.05, 133.88, 138.73, 139.59, 142.66, 145.60, 192.01; MS (MALDI-TOF): *m/z* calcd for $C_{42}H_{50}O_2Si_2$: 643.33 $[M]^+$; found: 643.569 $[M]^+$; elemental analysis calcd (%) for $C_{42}H_{50}O_2Si_2$: C 78.45, H 7.84; found: C 78.65, H 7.93.

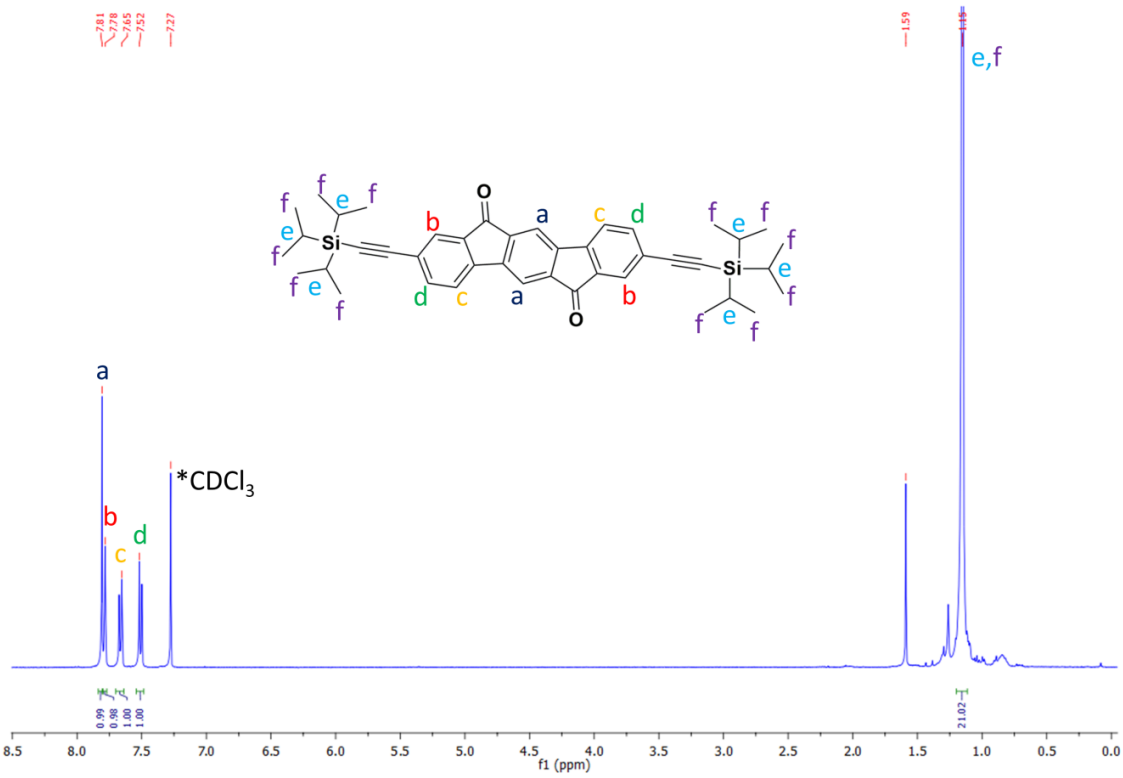

Figure 2.2.2.3.1 ^{1}H NMR spectra of **TIPS-IFDK** measured in $CDCl_3$.

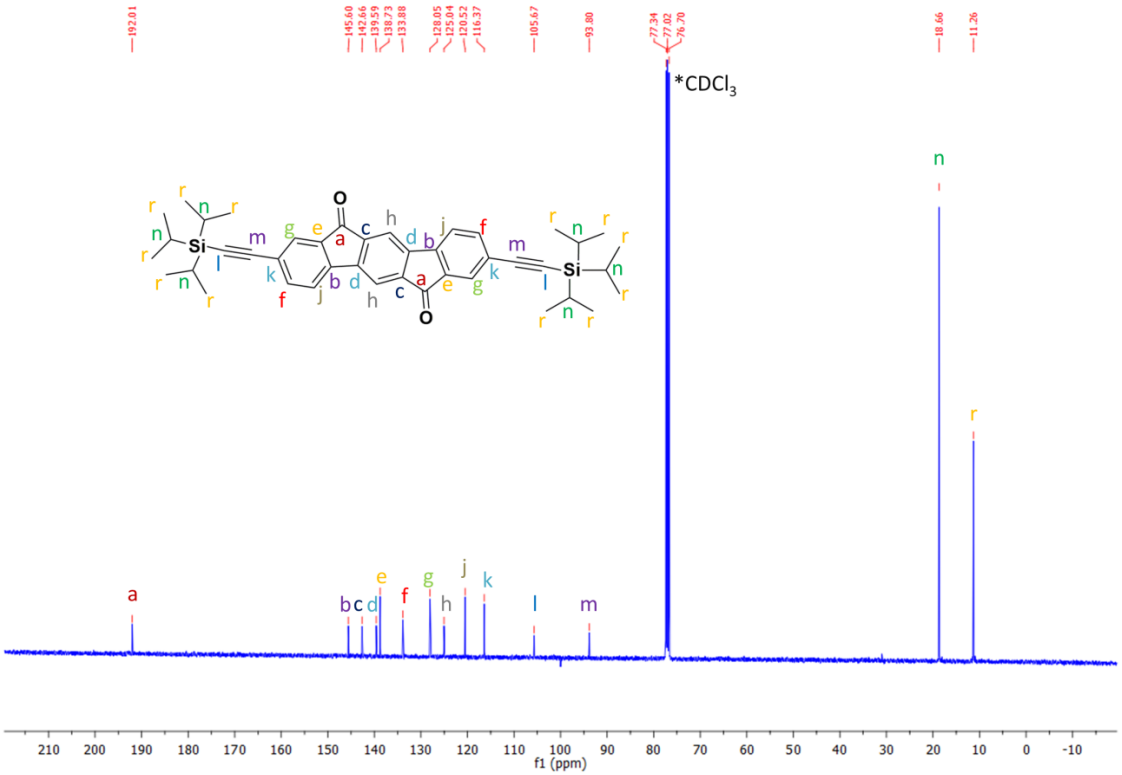

Figure 2.2.2.3.2 ^{13}C NMR spectra of **TIPS-IFDK** measured in $CDCl_3$.

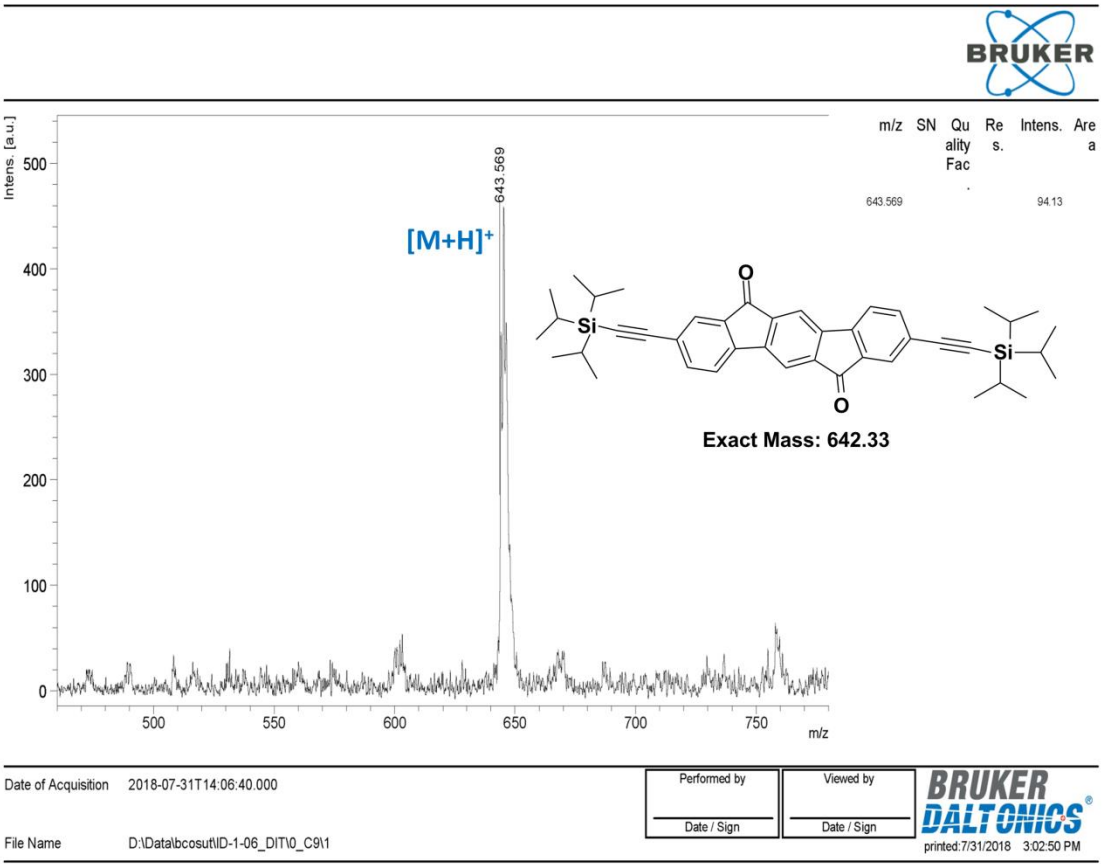

Figure 2.2.2.3.3 Positive ion and linear mode MALDI TOF-MS spectrum of **TIPS-IFDK**

2.2.2.4 **2,2'-(2,8-bis((triisopropylsilyl)ethynyl)indeno[1,2-b]fluorene-6,12-diylidene)dimalononitrile (TIPS-IFDM)**

A mixture of 2,8-bis((triisopropylsilyl)ethynyl)indeno[1,2-b]fluorene-6,12-dione (TIPS-IFDK) (0.400 g, 0.622 mmol) and malononitrile (0.575 g, 8.71 mmol) was dissolved in dry chlorobenzene (50 mL) under nitrogen, and stirred at 35°C for 15 min. Afterward, pyridine (0.935 g, 11.818 mmol) and $TiCl_4$ (1.180 g, 6.22 mmol) were added into reaction mixture. After addition, the resulting mixture was heated and stirred at 110 °C for 5 h under nitrogen. After completing reaction, the reaction mixture was allowed to cool down to room temperature, and quenched with water. The reaction mixture was extracted with chloroform, dried with Na_2SO_4, filtered and concentrated to get the crude product as dark brown solid. The crude was then purified through column chromatography on silica gel using $CHCl_3$:Hexane (1:1) as mobile phase to afford the final product as a black solid. (0.386 g, 84% yield). ^{1}H NMR (400 MHz, $CDCl_3$), δ (ppm): 1.16 (s, 42H), 7.58 (d, *J*=8.0 Hz, 2H), 7.65 (d, *J*=8.0 Hz, 2H), 8.49 (s, 2H), 8.56 (s, 2H); ^{13}C NMR (100 MHz, $CDCl_3$): δ (ppm): 11.25, 18.66, 78.98, 95.20, 105.16, 112.40, 118.45, 120.96, 125.63, 130.31, 134.06, 138.64, 139.26, 140.04, 142.98, 158.84; MS (MALDI-TOF): *m/z* calcd for $C_{48}H_{50}N_4Si_2$: 739.36 $[M]^+$; found: 739.397 $[M]^-$; elemental analysis calcd (%) for $C_{48}H_{50}N_4Si_2$: C 78.00, H 6.82, N 7.58; found: C 78.17, H 6.84, N 7.49.

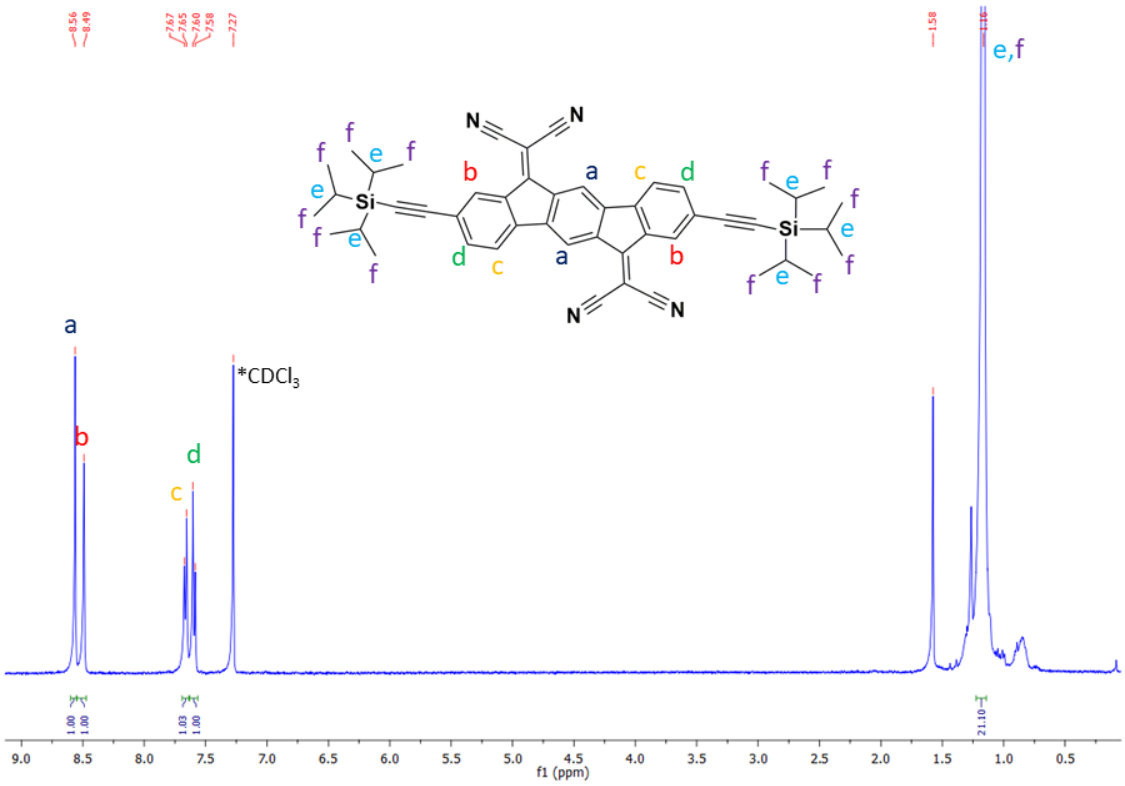

Figure 2.2.2.4.1 ^{1}H NMR spectra of **TIPS-IFDM** measured in $CDCl_3$.

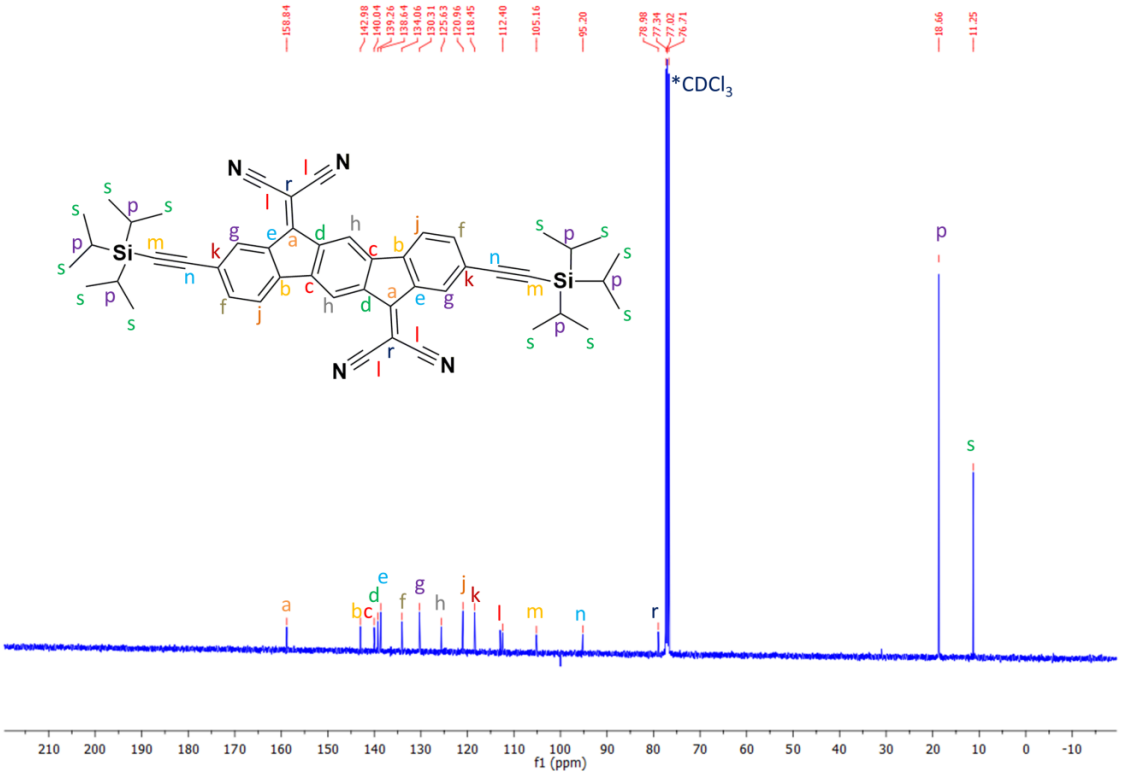

Figure 2.2.2.4.2 ^{13}C NMR spectra of **TIPS-IFDM** measured in $CDCl_3$.

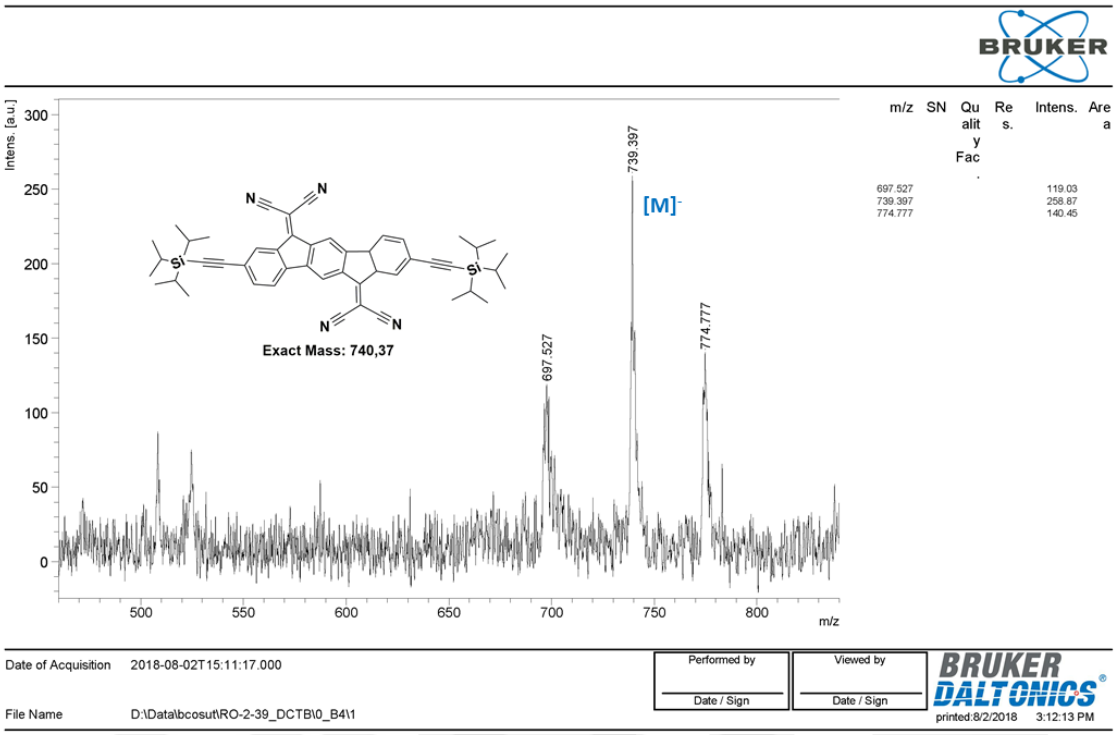

Figure 2.2.2.4.3 Negative ion and linear mode MALDI TOF-MS spectrum of **TIPS-IFDM**

2.2.3 Device Fabrication and Characterization

For the fabrication of top-contact/bottom-gate (TC/BG) OFETs, highly *n*-doped silicon wafers with a 300 nm thermally grown SiO_2 gate dielectric were used as device substrates. The substrates were cleaned via sonication in 2-propanol for 15 min, followed by oxygen plasma cleaning for 5 min (Harrick plasma, PDC-32G, 18 W). A general procedure was employed for PS-brush (M.W. = 19500 or 28000 g mol^{-1}) treatment onto the gate dielectric layers.[64–66] Thin films of semiconducting layers were fabricated via solution-shearing.[67–69] During the solution-shearing process, various parameters such as solvent type (toluene, chlorobenzene, 1,2-dichlorobenzene, chloroform), semiconductor solution concentration (1-8 mg/mL), shearing speed (1-8 mm/min), substrate temperature (~ 50-65 % of the boiling point of solvent), and thermal annealing temperature (75-85 °C) were optimized. Thicknesses of the semiconductor thin-films were measured with a profilometer (DEKTAK-XT, Brucker). The Au electrodes (40 nm) were thermally evaporated under high vacuum (deposition rate = 0.2 Å·s^{-1}) yielding various channel lengths (L = 50 and 100 μm) and widths (W = 500 and 1000 μm). The current–voltage characteristics of the fabricated OFETs were measured using a Keithley 4200 SCS at room temperature under vacuum or in ambient. The saturation mobility (μ_{sat}) was calculated using the formula:

$$\mu_{sat} = (2I_{DS}L)/[WC_i(V_G-V_{th})^2] \mu_{sat} = (2I_{DS}L)/[WC_i (V_G - V_{th})^2]$$

where I_{DS} is the source-drain current, L is the channel length, W is the channel width, C_i is the areal capacitance of the gate dielectric, V_G is the gate voltage, and V_{th} is the threshold voltage. The surface morphology and microstructure of thin-films were characterized by atomic force microscopy (AFM, NX10, Park systems) and X-ray diffraction (XRD, Smartlab, Rigaku) techniques, respectively.

2.3 RESULTS AND DISCUSSIONS

2.3.1 Synthesis, single-crystal structures and thermal characterizations.

The synthesis of **TIPS-IFDK** and **TIPS-IFDM** small molecules are shown in Figure 2.3.1.1, which involves a high-temperature Sonogashira cross-coupling reaction as the key step to introduce (trialkylsilyl)ethynyl units. The experimental conditions employed for the synthesis of the intermediate indenofluorene compound **IFDK-Br$_2$** was the same as previously reported by us.[70–72] In the first step, a highly selective Suzuki cross-coupling was carried out between methyl 5-bromo-2-iodobenzoate and 1,4-benzenediboronic acid bis(pinacol) ester compounds in the presence of $Pd(PPh_3)_4$ catalyst to give **1** in 91% yield. The observed high yield at each reaction site (95.4% yield) and the great selectivity on -I substituent are attributed to the presence of electron-withdrawing ester group positioned *ortho* to -I and higher reactivity of –I in Suzuki cross-couplings as compared to –Br.[73,74] Then, double intramolecular Friedel-Crafts acylation was carried out in concentrated H_2SO_4 at 120 °C to afford the ladder-type indenofluorene intermediate **IFDK-Br$_2$**. The yield obtained for this ring closure is 90% and it shows the formation of only indeno[1,2-b]fluorene-6,12-dione isomer. Note that although **IFDK-Br$_2$**'s insolubility prevents structural characterization with $^1H/^{13}C$ NMR, the following Sonogashira cross-coupling reaction yields highly soluble IFDK-derivatives that could be characterized by $^1H/^{13}C$ NMR spectroscopy. In the Sonogashira cross-coupling reaction of **IFDK-Br$_2$**, column chromatography yielded only indeno[1,2-*b*]fluorene-6,12-dione-based **TIPS-IFDK** compound; no by-product having indeno[2,1-*a*]fluorene-11,12-dione isomer was isolated. This indicates a very high selectivity in the second intramolecular acylation step. A primitive mechanistic analysis of this reaction according to valence bond theory demonstrate that there is no resonance stabilization effect between –*ortho* and –*para* acylations (Figure 2.3.1.2). Therefore, considering that the reaction was carried out at high temperature, thermodynamic effects are present and it's very likely that the difference in the energetics of the formation of transition state and/or the product between two isomers is

the key factor.[75,76] This is very consistent with the previous reports of indeno[2,1-*a*]fluorene-11,12-dione derivatives in the literature that they were all prepared from 1,2-benzene-diacid/diester precursors which synthetically allows the formation of only indeno[2,1-*a*]fluorene-11,12-dione isomer.[77,78] **IFDK-Br$_2$** has a very low solubility in organic solvents, preventing any solution-based convenient purification. So, this compound was directly used in the following cross-coupling step without any further purification. Next, in the presence of CuI/Pd(PPh$_3$)$_2$Cl$_2$ cocatalyst/catalyst system and Et$_3$N base, (triisopropylsilyl)ethynyl groups are added at 2,8-positions by reacting **IFDK-Br$_2$** with (triisopropylsilyl)acetylene. **TIPS-IFDK** was obtained in 64% yield. Although most of the previous studies on (trialkylsilyl)ethynyl-substituted semiconductors have focused on π-extensions in the short molecular axis (Figure 2.3.1.3),[49–51,79–83] herein the molecular π-core is extended along the long molecular axis. This unique design allows us to maintain the electron-withdrawing carbonyl/dicyanovinylene functionalities in the final small molecules with no σ-insulating alkyl substituents nearby, and it helps us to understand whether (trialkylsilyl)ethynyl functionalization in the long molecular axis could yield as effective solid-state packing as those observed in the molecules extended along their short molecular axis. Subsequent Knoevenagel condensation of **TIPS-IFDK** to form dicyanovinylene-substituted **TIPS-IFDM** was achieved in 84% yield using excess malononitrile with pyridine base and TiCl$_4$ Lewis acid. In contrast to the poor solubility of the parent compound **IFDK-Br$_2$**, new small molecules **TIPS-IFDK** and **TIPS-IFDM** were found to be freely soluble in common organic solvents ($CHCl_3$, CH_2Cl_2, THF, and toluene). As a result, they were conveniently purified by silica gel column chromatography. The purities and structures of the intermediate compounds and final small molecules were characterized by ^{1}H/^{13}C NMR (Figure 2.2.2.3.1, 2.2.2.3.2, 2.2.2.4.1, and 2.2.2.4.2), elemental analysis, mass spectroscopy (MALDI-TOF) (Figure 2.2.2.3.3 and 2.2.2.4.3), ATR-FTIR (Figure 2.3.1.4), and melting point measurements. In order to perform a comparative optoelectronic properties study between new molecules and their β-substituted counterparts, **β-DD-TIFDKT** and **β-DD-TIFDMT** reference compounds were synthesized in accordance with our previously reported procedure.[84]

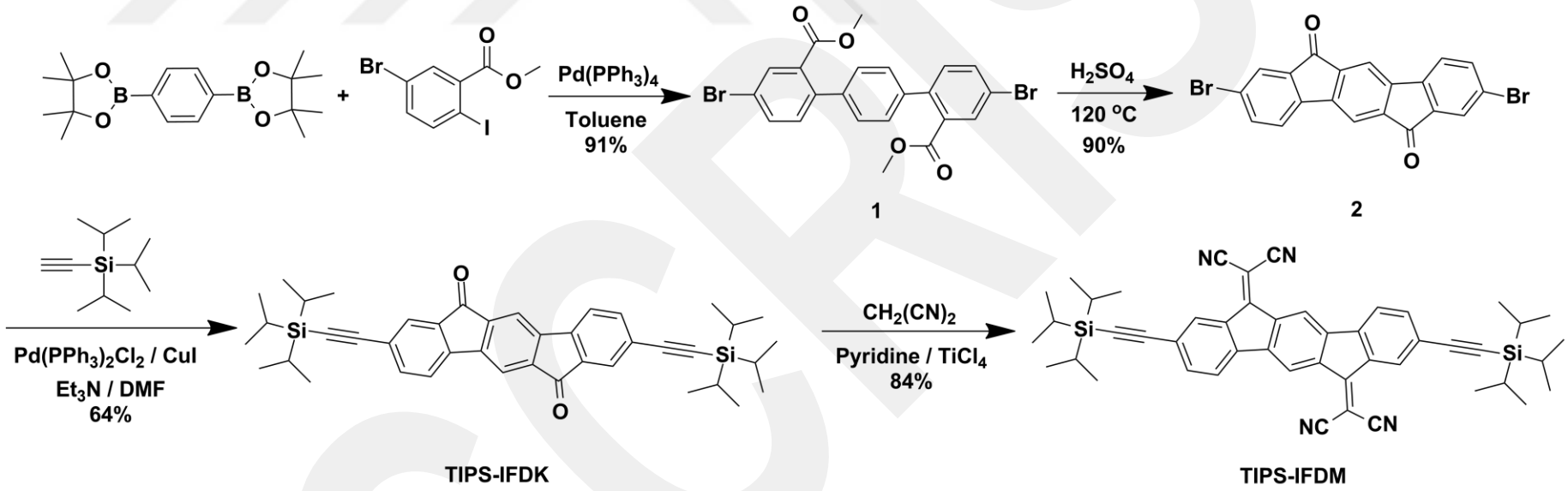

Figure 2.3.1.1 Synthetic routes to **TIPS-IFDK** and **TIPS-IFDM**

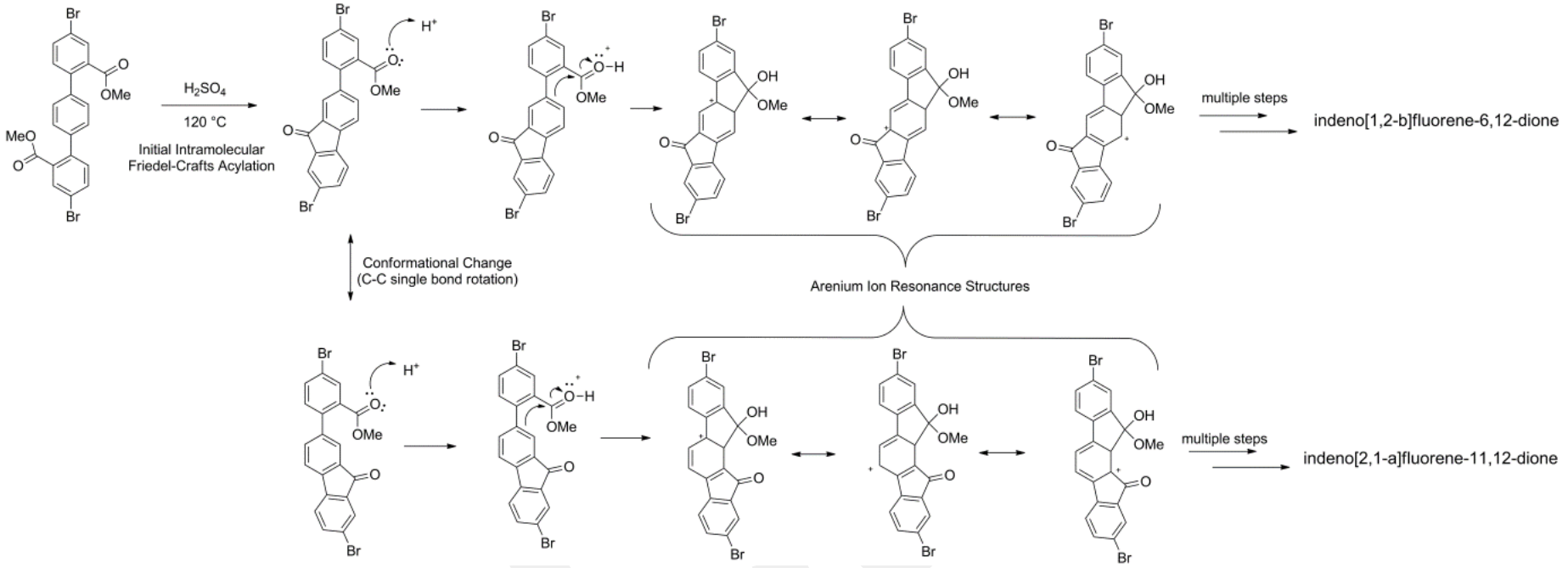

Figure 2.3.1.2 Proposed mechanisms for the second intramolecular Friedel-Crafts acylation reaction in the formation of indeno[2,1-a]fluorene-11,12-dione and indeno[1,2-b]fluorene-6,12-dione isomers showing plausible arenium resonance structures.

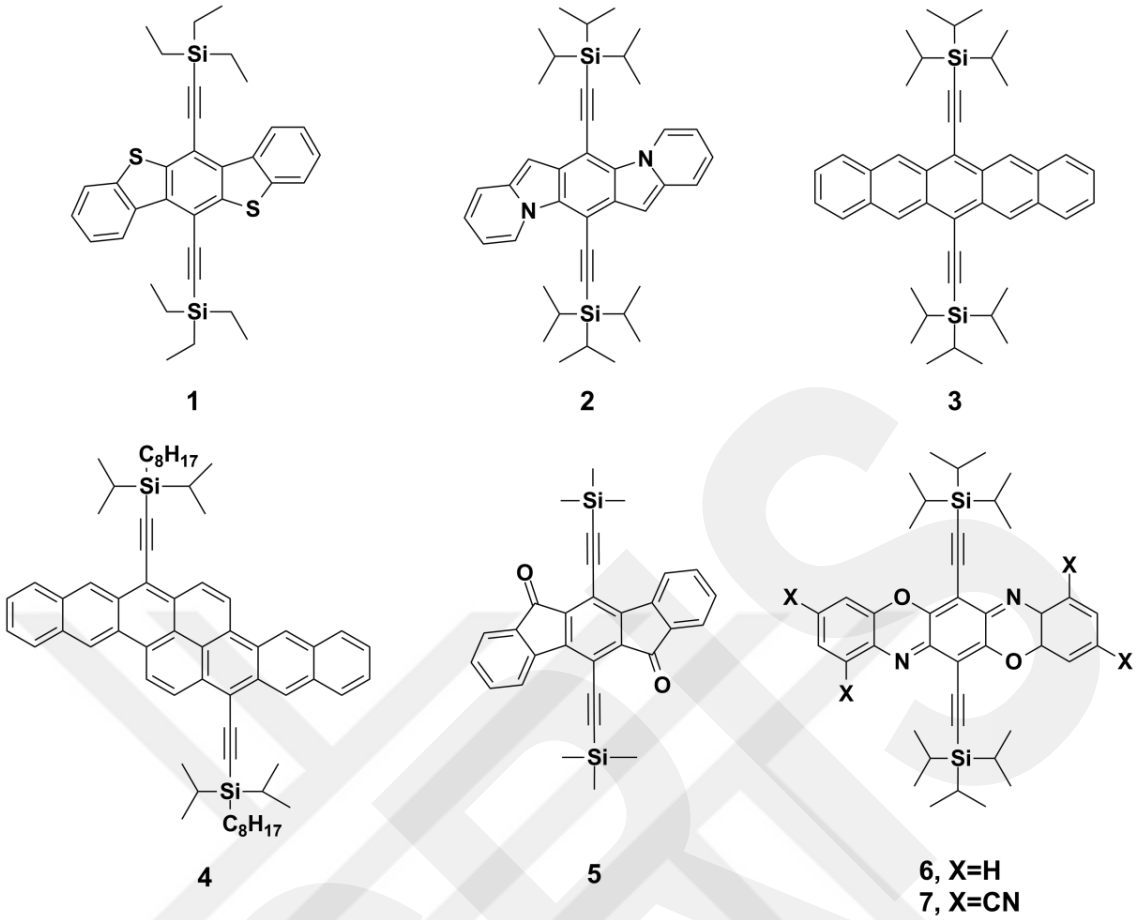

Figure 2.3.1.3 Chemical structures of representative molecular semiconductors 1[81], 2[81], 3[50,51,79,81], 4[85], 5[49], 6[83], and 7[82] substituted with (trialkylsilyl)ethynyl units on their short molecular axis.

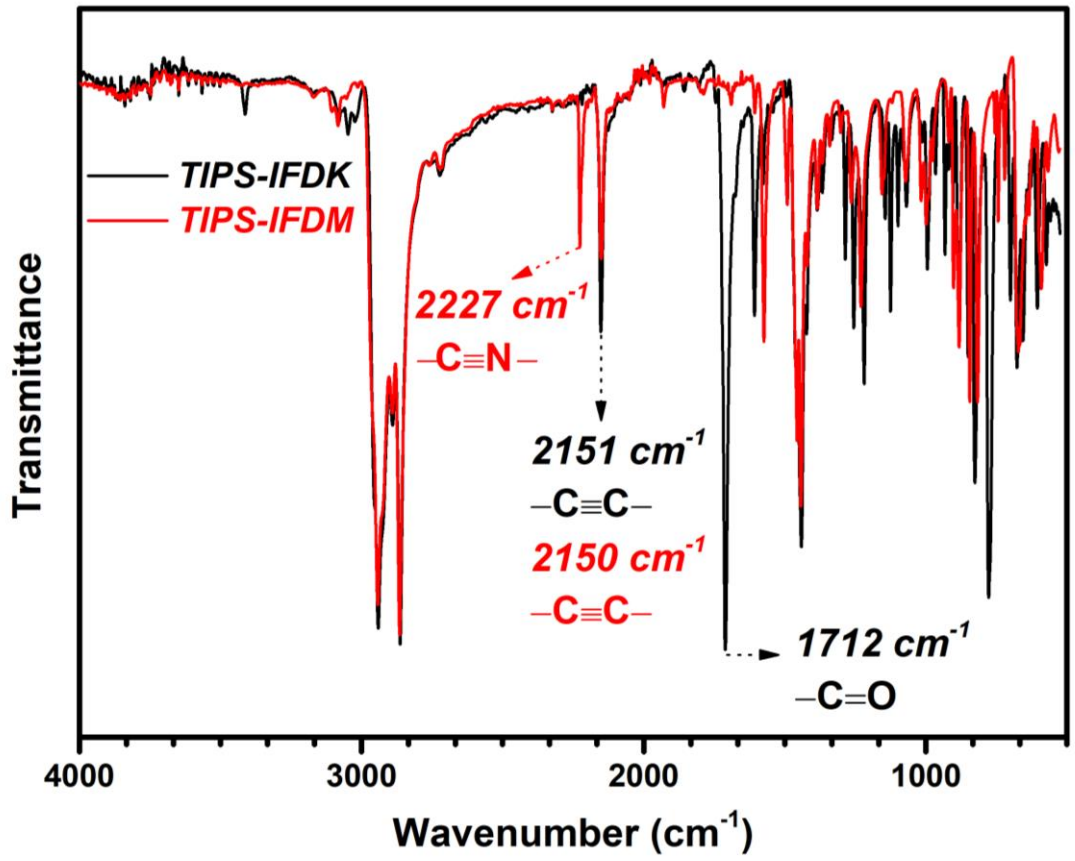

Figure 2.3.1.4 ATR FTIR Spectra of the semiconductors **TIPS-IFDK** and **TIPS-IFDM** showing important stretching vibrational peaks.

As shown in Figure 2.3.1.5, both small molecules were found to be thermally very stable with thermolysis onset temperatures (5% weight loss) of 400 °C (for **TIPS-IFDM**) and 420 °C (for **TIPS-IFDK**). Two-step decomposition profiles were observed for both small molecules with small steps at ≈90-92% of the original weights, which correspond to the mass losses of methyl ($-CH_3$) and/or isopropyl ($-CH(CH_3)_2$) substituent(s) in the trialkylsilyl end units. Based on differential scanning calorimetry measurements, **TIPS-IFDM** show two endothermic peaks at 280 °C (enthalpy = 3.55 J g^{-1}) and 315 °C (enthalpy = 22.09 J g^{-1}). The thermal transition at 315 °C was later confirmed by conventional melting-temperature measurement to agree with the melting point of **TIPS-IFDM** (T_{mp} = 316-317 °C). The low-enthalpy thermal transition at 280 °C prior to the melting could be attributed to solid-to-liquid crystal transition, which is not unusual for rod-shaped π-conjugated molecules.[71,86,87] A corresponding exothermic crystallization peak was observed at 285 °C (enthalpy = 23.05 J g^{-1}) in the cooling cycle. The melting temperature of **TIPS-IFDM** is much higher (ΔT_{mp} = 70-80 °C) than those of previously reported similar sized alkyl-thienyl substituted IFDM derivatives indicating the efficiency of this new design to promote strong solid-state packing with low density of flexible alkyl substituents.[70,71,84] Despite the presence of endothermic thermal transitions at 176 °C (enthalpy = 15.14 J g^{-1}) and 242 °C (enthalpy = 6.94 J g^{-1}) for **TIPS-IFDK** in DSC profile, no observable melting (solid-to-isotropic liquid) process occurred before decomposition at >380 °C. Therefore, the observed thermal processes could be attributed to solid-to-solid or solid-to-liquid crystal transitions. Note that, as compared with previously developed alkyl thienyl-substituted IFDK derivatives, the absence of long and flexible alkyl substituents tune intermolecular interactions and result in complete disappearance of the melting process. And, this is very comparable to the thermal behavior of the parent carbon substituted **IFDK-Br_2** compound, which is most likely a result of structurally close molecular frameworks and similar solid-state packing motifs (*vide infra*).

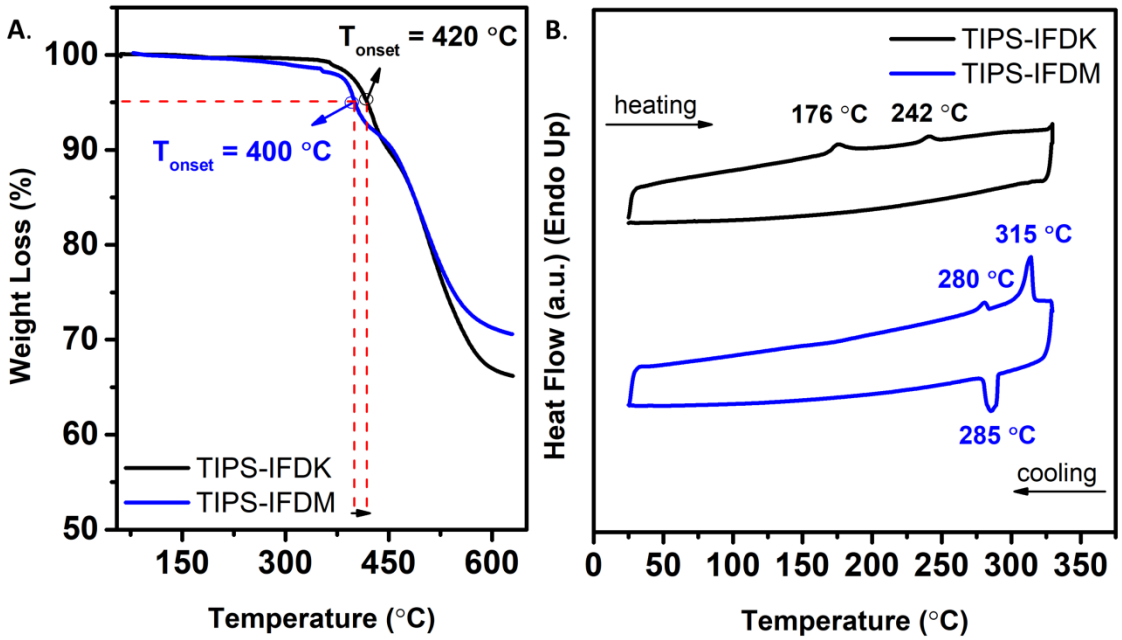

Figure 2.3.1.5 Thermogravimetric analysis (TGA) curves (A) and differential scanning calorimetry (DSC) measurement curves (B) of **TIPS-IFDK** and **TIPS-IFDM** at a temperature ramp of 10 °C min^{-1} under N_2.

In order to get a better insight into the intermolecular interactions in the solid state, compounds **TIPS-IFDK** and **TIPS-IFDM** were further characterized by X-ray crystallography (Figs. 2.3.1.6.A, 2.3.1.7.A). The plate-like single crystals of **TIPS-IFDK** and **TIPS-IFDM** were obtained by diffusion of hexane into a tetrahydrofurane (THF) solution at room temperature. **TIPS-IFDK** crystallizes in the triclinic space group *P*-1 while **TIPS-IFDM** crystallizes in the monoclinic *C*2/*c* space group. The structure analysis reveals that the substantially planar π-conjugated backbones of **TIPS-IFDK** and **TIPS-IFDM** are found lying across an crystallographic inversion center. The core planarity of **TIPS-IFDK** is perfectly matching with IFD-based structures reported in Cambridge Structural Database (CSD Ref. Codes, EWEKAT, EWEKEX, EWEKIB, SUVLEC, ZEGNUX, ZEGPAF, ZEGPEJ)[49,54,70] while core planarity of **TIPS-IFDM** is quite different from the that of 2,2'-(2,8-Dibromo-5,11-didodecylindeno[1,2-b]fluorene-6,12-diylidene)dimalononitrile (CSD Ref. Code: KUCBAM) reported in literature.[55] For **TIPS-IFDK**, the short CH···O contacts (O1···H8 = 2.541 Å) between the adjacent molecules construct one-dimensional chain structure along the crystallographic *a*-axis (Fig. 2.3.1.6.C). These one-dimensional chains are further expanded into a two-dimensional π-layers in a brick-wall packing arrangement with a favorable interplanar distance of 3.416 Å (Figs 2.3.1.6.B and 2.3.1.6.D). As in our previously reported structure[70], the presence of strong local dipoles of carbonyl (–C=O) groups can overcome the formation of edge-to-face aromatic interactions (C/H···π), and results in the π-stacking in a parallel-displaced conformation, which ensure the availability of electrons as potential charge carriers. When the dicyanovinylene (-C=$(CN)_2$) substituents are used instead of carbonyl groups, the one-dimensional chains formed by CH···N interactions (N2···H14 = 2.458 Å, 2.3.1.7.C) are further expanded into a 2D layers. However, the π-system of **TIPS-IFDM,** which is different from the that of **TIPS-IFDK**, is found to be one-dimensional slipped-π-stacked arrangement (2.3.1.7.D) with a favorable interplanar distance of 3.469 Å (2.3.1.7.B).

XRD data were obtained with Bruker APEX II QUAZAR three-circle diffractometer. Indexing was performed using APEX2 [APEX2, version 2014.11-0, Bruker (2014), Bruker AXS Inc., Madison, WI]. Data integration and reduction were carried out with SAINT [SAINT, version 8.34A, Bruker (2013), Bruker AXS Inc., Madison, WI]. Absorption correction was performed by multi-scan method implemented in SADABS [SADABS, version2014/5, Bruker (2014), Bruker AXS Inc., Madison, WI.]. The structure was solved using SHELXT[88] and then refined by full-matrix least-squares refinements on F^2 using the SHELXL[89] in SHELXTL Software Package [Bruker, SHELXTL, version 6.14, Bruker AXS Inc., Madison, Wisconsin, USA, 2010]. All non-hydrogen atoms were refined anisotropically using all reflections with $I > 2\sigma(I)$. Aromatic and aliphatic C-bound H atoms were positioned geometrically and refined using a riding mode. Crystallographic data and refinement details of the data collection for compounds **TIPS-IFDK** and **TIPS-IFDM** are given in Table 2.3.1.1 Crystal structure validations and geometrical calculations were performed using Platon software.[90,91] Mercury software[92] was used for visualization of the cif files. Additional crystallographic data with CCDC reference numbers 1854236 (**TIPS-IFDK),** 1854237 (**TIPS-IFDM)** have been deposited within the Cambridge Crystallographic Data Center.[93]

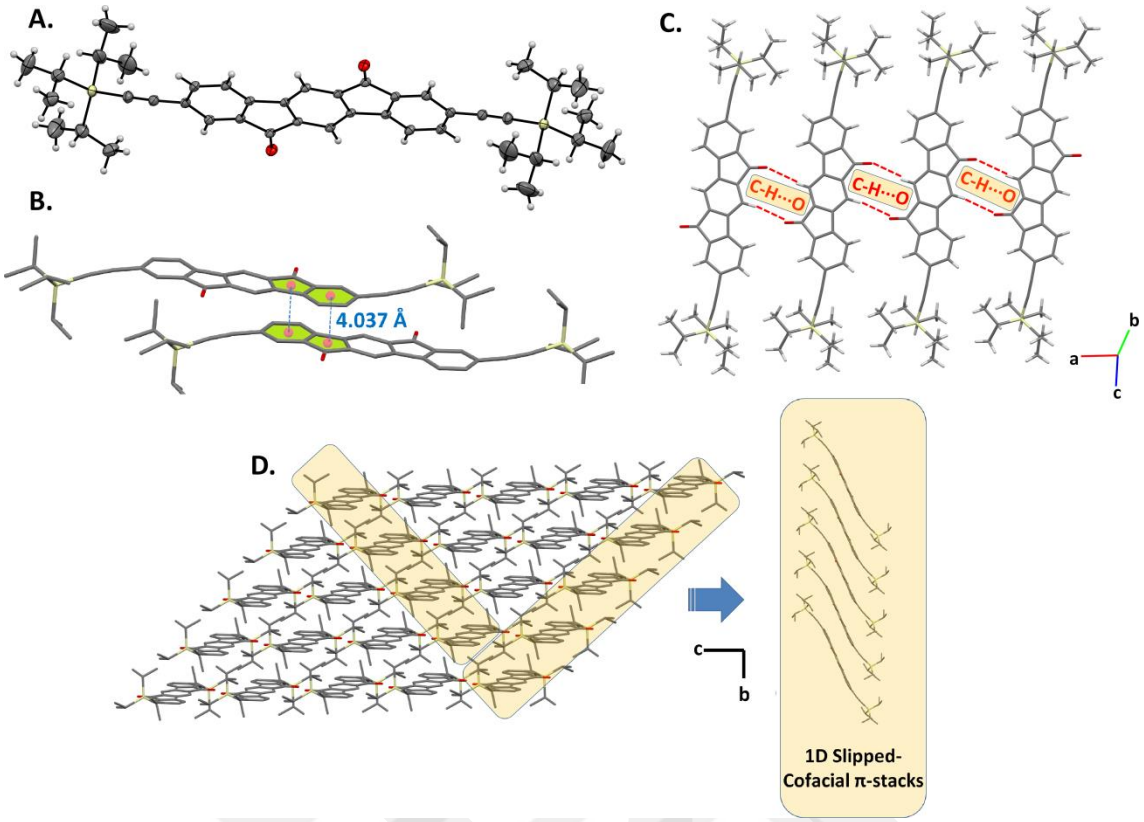

Figure 2.3.1.6 ORTEP drawings of the crystal structure of **TIPS-IFDK** (30% probability level) (A), representations of pairs of indeno[1,2-b]fluorene-6,12-dione (**IFDK**) molecules arranged in a slipped π-stacked fashion with a centroid-to-centroid distance of 4.037 Å (B), the continuous π-layer formation via short CH···O contacts (C), perspective views of the molecular arrangement and one-dimensional cofacial slipped π-stacks (D).

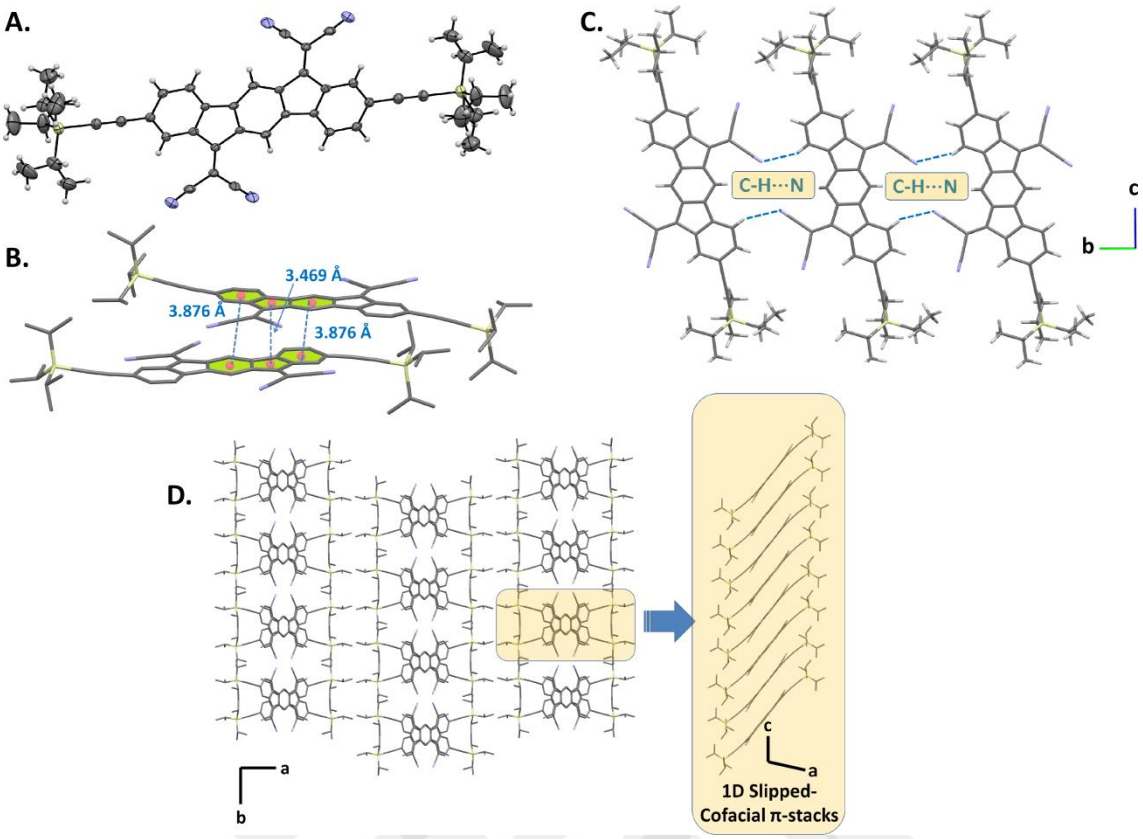

Figure 2.3.1.7 ORTEP drawings of the crystal structure of **TIPS-IFDM** (30% probability level) (A), representations of pairs of indeno[1,2-b]fluorene-6,12-diylidene)dimalononitrile (**IFDM**) molecules arranged in a slipped π-stacked fashion with favorable π···π distances of 3.469/3.876 Å (B), the continuous π-layer formation via short CH···N contacts (C), perspective views of the molecular arrangement and one-dimensional cofacial slipped π-stacks(D).

Table 2.3.1.1 Crystal data and refinement parameters for compounds **TIPS-IFDK** and **TIPS-IFDM**.

	TIPS-IFDK	**TIPS-IFDM**
CCDC	1854236	1854237
Empirical Formula	$C_{42}H_{50}O_2Si_2$	$C_{48}H_{50}N_4Si_2$
Formula weight (g. mol^{-1})	643.00	739.10
Temperature (K)	296(2)	296(2)
Wavelength (Å)	0.71073	0.71073
Crystal system	Triclinic	Monoclinic
Space group	*P*-1	*C*2/*c*
***a* (Å)**	7.6019(6)	39.755(5)
***b* (Å)**	7.7795(7)	10.0294(12)
***c* (Å)**	17.7908(15)	11.4351(14)
α(°)	94.036(5)	90
β(°)	92.577(5)	102.874(8)
γ(°)	114.867(4)	90
Crystal size (mm)	0.04 x 0.36 x 0.47	0.03 x 0.32 x 0.41
***V* (Å^3)**	948.98(14)	4444.8(9)
Z	1	4
ρ_{calcd} (g. cm^{-3})	1.125	1.104
μ (mm^{-1})	0.126	0.115
***F*(000)**	346	1576
θ range for data collection (°)	2.96 -25.00	2.10 - 25.03
h*/*k*/*l	-9<=h<=9, -9<=k<=9, -21<=l<=21	-37<=h<=47, -11<=k<=11, -13<=l<=10
Reflections collected	13766	16272
Independent reflections	3303 [R(int) = 0.0573]	3918 [R(int) = 0.0967]
Data/restraints/parameters	3303 / 0 / 214	3918 / 19 / 250
Goodness-of-fit on F^2 (S)	1.078	1.016
Final *R* indices [$I > 2\sigma(I)$]	R_1 = 0.0860, wR_2 = 0.2596	R_1 = 0.1097, wR_2 = 0.3031
***R* indices (all data)**	R_1 = 0.0982, wR_2 = 0.2746	R_1 = 0.2020, wR_2 = 0.3730
Largest diff. peak and hole (e.Å^{-3})	0.978 and -0.381	0.414 and -0.234

2.3.2 Optical and Electrochemical Properties

Density functional theory calculations for **TIPS-IFDK** and **TIPS-IFDM**, along with the previously developed reference semiconductors **β-DD-TIFDKT(M)** (Figure 2.1.1), were performed using B3LYP method and 6-31G** basis set. The calculations reveal that the present (trialkylsilyl)acetylene functionalization decreases both HOMO and LUMO energies relative to the previously developed β-derivatives (Figure 2.3.2.1.C). Analysis of the orbital spatial distributions shows that while there is significant HOMO wave-function density on ethynyl units, LUMOs are delocalized only in the central indenofluorene π-units. Thus, LUMO stabilization could only be attributed to the positive (electron-withdrawing) inductive effect of sp-hybridized ethnyl (-C=C-) end units as compared with relatively electron-rich thienyl units. This also clearly explains that the energetic stabilization of HOMOs (ΔE = -0.15 - -0.19 eV) are larger than those of LUMOs (-0.04 - -0.1), which results in increased HOMO-LUMO gaps (ΔE = 0.1-0.2 eV) in the new TIPS-substituted molecules. Note that increased band-gaps are also the result of changing donor-acceptor-donor π-architecture to a fully π-acceptor architecture. Solution-processable small molecules with low LUMO/HOMO levels are very attractive materials as non-fullerene acceptors in BHJ-OPVs, since, when combined with donor materials, they yield efficient exciton dissociation via only electron-transfer without any undesired hole-transfer. In addition, acceptor materials with stabilized HOMO energies allow the use of extended types of donor materials with low HOMO energies.

The UV-vis absorption spectra of the present compounds **TIPS-IFDK** and **TIPS-IFDM** were measured in dichloromethane solutions and as spin-coated thin-films (Figure 2.3.2.1.A/2.3.2.1.B and Table 2.3.2.1). At short wavelengths (<400 nm) both compounds exhibit well-defined peaks with intense absorptions corresponding to the π-π* transition of the diethnyl-subtituted indeno[1,2-*b*]fluorene π-core. The low-intensity peaks at 514 nm (for **TIPS-IFDK**) and 625 nm (for **TIPS-IFDM**) are attributed to symmetry forbidden n-π* transitions as a result of the presence of carbonyl/dicyanovinilene functional groups. Despite negligible changes at high-energy

absorption peaks (<400 nm), the effect of carbonyl *vs* dicyanovinylene substitution is evident in the low-energy absorption peaks that significant bathochromic shift of ~111 nm was observed going from carbonyl to dicyanovinylene on the methylene bridges. This is apparently the result of LUMO energetic stabilization (*vide infra*) due to the stronger electron-withdrawing ability of dicyanovinylene and further extended delocalization of LUMO wavefunction on dicyanovinylene units. The optical band gaps estimated from the low-energy absorption edge onsets are 2.12 eV for **TIPS-IFDK** and 1.66 eV for **TIPS-IFDM**. Consistent with the DFT calculations, both compounds showed hypsochromically shifted low-energy peaks ($\Delta\lambda$ = 16-56 nm) and increased optical band gaps when compared with their β-substituted counterparts ($E_{g(\beta\text{-DD-TIFDKT})}$ = 2.02 eV and $E_{g(\beta\text{-DD-TIFDKT})}$ = 1.53 eV) (Figure 2.3.2.1.A). When going from solution to spin-coated thin films, both compounds exhibit bathochromic shifts in the local absorption maxima with almost no changes in the low-energy absorption onsets. This indicates that although the presence of intermolecular interactions in the solid state affects the intensity of plausible optical transitions, it does not have any effect on the minimum energy gap. Note that this is very different than those of previously reported alkylthienyl-substituted D-A-D type indenofluorene derivatives, which typically showed reduced band gaps as a result of molecular backbone planarization in the solid-state.[55] The lack of the same kind of backbone planarization in the present molecules due to the nature of their π-structures explains the minimal changes in their optical band gaps.

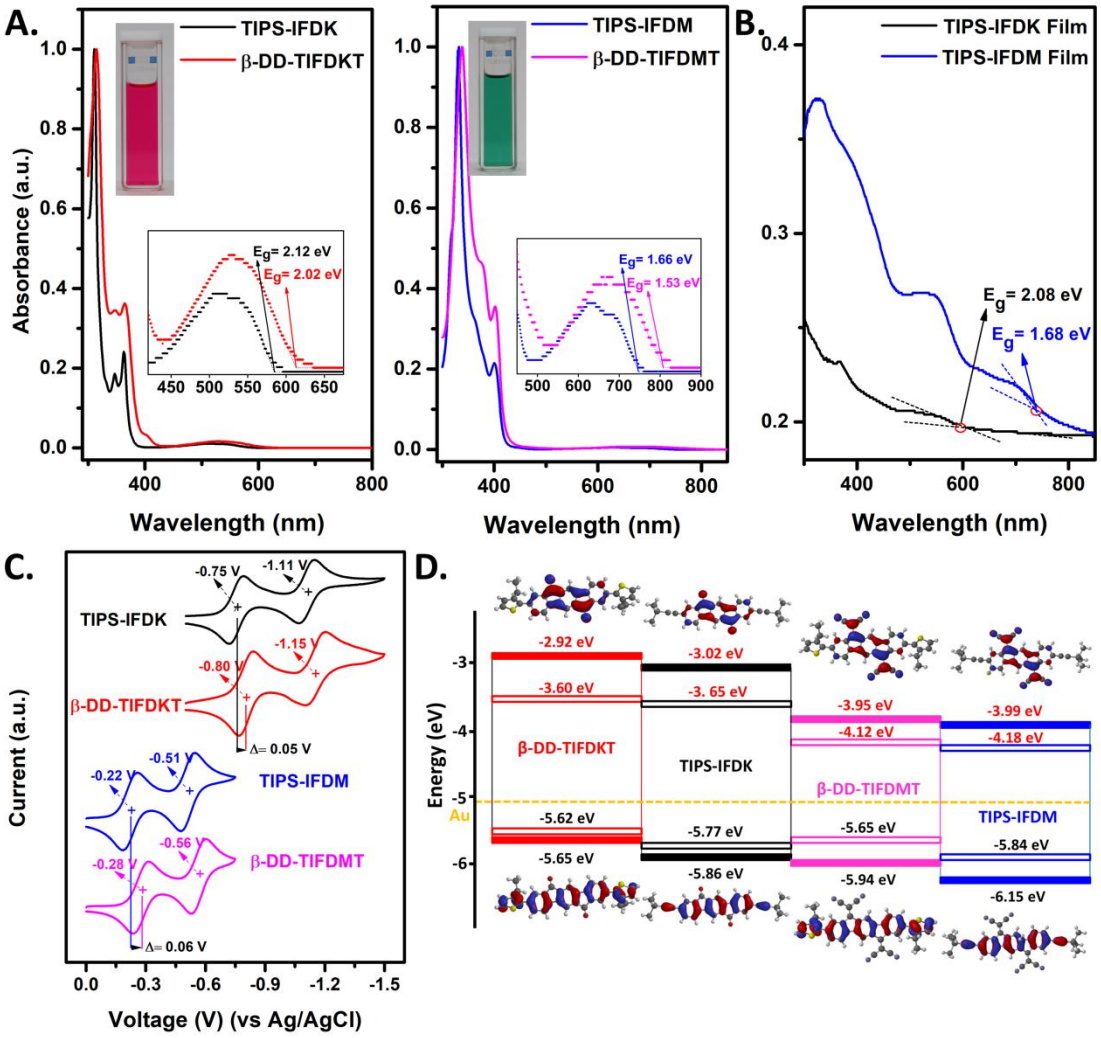

Figure 2.3.2.1. For **TIPS-IFDK** and **TIPS-IFDM**, and the reference molecules **β-DD-TIFDKT** and **β-DD-TIFDMT**, optical absorption in dichloromethane solution (insets are the images of the corresponding TIPS-IFDK(M) solutions) (A), optical absorption as thin-films (B), cyclic voltammograms in dichloromethane (0.1 M $Bu_4N^+PF_6^-$, scan rate = 50 mVs^{-1}) (C), and calculated (solid blocks; DFT/B3LYP/6-31G**) and experimental (hollow blocks) HOMO and LUMO energy levels with topographical orbital representations (D).

The electrochemical properties of the new compounds **TIPS-IFDK/TIPS-IFDM** and reference compounds **β-DD-TIFDKT/β-DD-TIFDMT** were investigated by cyclic voltammetry technique in the exact same experimental condition to study the small changes in the frontier orbital energetics. As shown in 2.3.2.1.C, both compounds showed reversible reduction peaks with the first half-wave potential located at -0.75 V (*vs Ag/AgCl*) for **TIPS-IFDK** and -0.22 V (*vs Ag/AgCl*) for **TIPS-IFDM**, which indicates redox stable *n*-doping characteristics. No electrochemical oxidation peak was observed for both small molecules. Since the electron-accepting ability of dicyanovinylene is greater than carbonyl and diethynyl-indenofluorene π-core remains the same, the reduction peaks exhibit significant anodic shifts (-0.75/-1.11 V → -0.22/-0.51 V) going from **TIPS-IFDK** to **TIPS-IFDM**. Additionally, when two small molecules with the same functionalities are compared, the half-wave-reduction potentials are found to be less negative for the new TIPS-substituted compounds relative to the reference compounds. This is obviously the result of the existence of electron-withdrawing ethynyl groups and the absence of electron-rich alkylthienyl units at 2,8-positions of the new molecules. The HOMO/LUMO energy levels were estimated as -5.77/-3.65 eV for **TIPS-IFDK** and -5.84/-4.18 eV for **TIPS-IFDM**, which are both lower than those of the parent **β-DD-TIFDKT** and **β-DD-TIFDMT** compounds. As shown in Figure 2.3.2.1.D, the energetic trends of the corresponding frontier molecular orbitals show great agreement between DFT calculations and experimental estimations. It is very encouraging for future materials design in indenofluorenes that even subtle changes measured in frontier molecular orbital energies could be predicted beforehand by density functional theory. Note that the LUMO energies of the new compounds are in the range of previously reported *n*-type semiconductors. Specifically, the LUMO energy level of **TIPS-IFDM** could enable air-stable *n*-channel conduction in OFETs.

Table 2.3.2.2 Summary of optical absorption/electrochemical properties and corresponding estimated frontier molecular orbital energies for new small molecules **TIPS-IFDK** and **TIPS-IFDM**, and reference molecules **β-DD-TIFDKT** and **β-DD-TIFDMT**.

Compound	$\lambda_{abs}^{sol.}$ (nm)[a]	$E_g^{sol.}$ (eV)[b]	λ_{abs}^{film} (nm)[c]	E_g^{film} (eV)[b]	$E_{1/2}^{red.}$ (V)[d]	E_{LUMO} (eV)[e]	E_{HOMO} (eV)[f]
TIPS-IFDK	312, 363, 514	2.12	369, 532	2.08	-0.75	-3.65	-5.77
β-DD-TIFDKT	315, 365, 530	2.02	365, 594[g]	1.89[g]	-0.80	-3.60	-5.62
TIPS-IFDM	329, 400, 625	1.66	329, 538, 693	1.68	-0.22	-4.18	-5.84
β-DD-TIFDMT	338, 401, 681	1.53	412, 759[g]	1.50[g]	-0.28	-4.12	-5.65

[a]From optical absorption measured in dichloromethane. [b]Optical band gap is estimated from the low-energy band edge of the corresponding UV-vis absorption spectrum. [c]From optical absorption measured as spin-coated thin-films on glass. [d]Recorded in 0.1 M $Bu_4N^+PF_6^-$ solution in CH_2Cl_2 at a scan rate of 50 mV/s using Pt working electrode and Ag/AgCl reference electrode. [e]Estimated from the equation: $E_{LUMO} = -4.40\ eV - E_{1/2}^{red.}$. [f]Calculated from: $E_g = E_{LUMO} - E_{HOMO}$. [g] Thin-film absorption data is taken from the reference.[55]

2.3.3 Thin-Film microstructure/morphology and field-effect transistor characterizations.

Charge-transport characteristics of the present semiconductors were studied in top-contact/bottom-gate (TC/BG) OFET devices under vacuum and in ambient. Thin-films of **TIPS-IFDM** (50 nm) and **TIPS-IFDK** (55 nm) were prepared by solution shearing semiconductor solutions in chlorobenzene (1.5 mg/ml) on PS (polystyrene)-brush coated n^{++}-Si/SiO_2 (300 nm) gate-dielectric substrates. This polymeric dielectric treatment was preferred to afford favorable semiconductor morphology/crystallization at the semiconductor-dielectric interface.[67,94] The microstructural and morphological properties of the semiconductor thin-films were studied by out-of-plane θ-2θ X-ray diffraction (XRD) and atomic force microscopy (AFM). As shown in Figure 2.3.3.1.A, for thin-films of **TIPS-IFDM** multiple sharp diffraction peaks of the same phase were observed indicating a highly crystalline semiconductor film with a high degree of solid-state ordering. The major diffraction peak was observed at 2θ = 4.67° (*d*-spacings of 1.9 nm) along with its higher degree peaks at 2θ = 9.30°, 13.92°, and 18.58°. Using the single-crystal unit cell parameters, simulation of the observed diffration pattern showed that molecules orient on the substrate having (200) crystal plane parallel to the surface (Figure 2.3.3.2.B). This indicates the formation of a "layer-by-layer" packing motif that consists of alternately packed semiconducting π-backbones and insulating trialkylsilyl substituents in the out-of-plane direction. In the semiconducting part, slipped π-π stacked molecules are aligned along the charge-transport direction (in-plane) with their π-cores tilted from the substrate normal ($\theta_{tilting}$ = 45°). This is also the result of having trialkylsilyl end-units, which favors to interact with the substrate surface and drives the molecular π-backbones to adopt edge-on orientations forming one-dimensional (1-D) slipped-stacked packing motif.[81,95] Each **TIPS-IFDM** molecule shows close π-π interactions with the neighboring two molecules involving its full indenofluorene π-system, which results in short π-π stacking distances of 3.47 Å between five-membered rings and 3.88 Å between six-membered rings. On the other hand, thin-films of **TIPS-IFDK** exhibit a low-intensity diffraction peak at 2θ = 5.09°

(*d*-spacings of 1.7 nm) along with its higher order peak at 2θ = 15.09°, which indicates a very limited crystallinity as compared to those of **TIPS-IFDM** (Figure 2.3.3.1.A). The simulation of the observed diffration pattern according to the single-crystal unit cell parameters showed that **TIPS-IFDK** molecules orient on the substrate having (001) crystal plane parallel to the surface (Figure 2.3.3.2.A). This also indicates a "layer-by-layer" packing motif having 1-D slipped π-π stacked molecules in the charge-transport direction. However, **TIPS-IFDK** molecules show increased tilting from the substrate normal ($\theta_{tilting}$ = 60°) and more limited π-π interactions, which involves part of the indenofluorene π-system and results in longer π-π stacking distances of 4.04 Å between five- and six-membered rings. Therefore, when two π-systems are compared in the present semiconductors, **IFDM** clearly shows more effective π-π stacking interactions with nearby molecules resulting in higher crystallinity and densely packed π-system in the charge-transport direction. Considering that the present semiconductor molecules share the exact same π-framework with only the difference of functional group, this undoubtedly reflects the effect of dicyanovinylene *vs* carbonyl functionalization. As shown in Figure 2.3.3.1.B, atomic force microscopy characterizations of the present semiconductor thin-films showed the formation of micrometer-sized ribbon-like domains aligned along the shearing directions. The surface of these ribbons appear to be very smooth over micrometer-sized areas indicating highly favorable two-dimensional molecular coverage on the surface during the solution-shearing process. On the basis of the step-height profile, a *layer-by-layer* semiconductor film growth mechanism was evident for **TIPS-IFDM** ribbons since step heights of ~2.2-2.3 nm matches well with the dimensions of the molecular layers show in Figure 2.3.3.2.B. In order to further elucidate the correlations between the observed microstructures and morphologies, the BFDH (Bravais, Friedel, Donnay and Harker) theoretical crystal morphologies for **TIPS-IFDK** and **TIPS-IFDM** were simulated, which predicted high aspect ratio crystal growths along the observed (200) and (001) crystal planes, respectively (Figure 2.3.3.3).

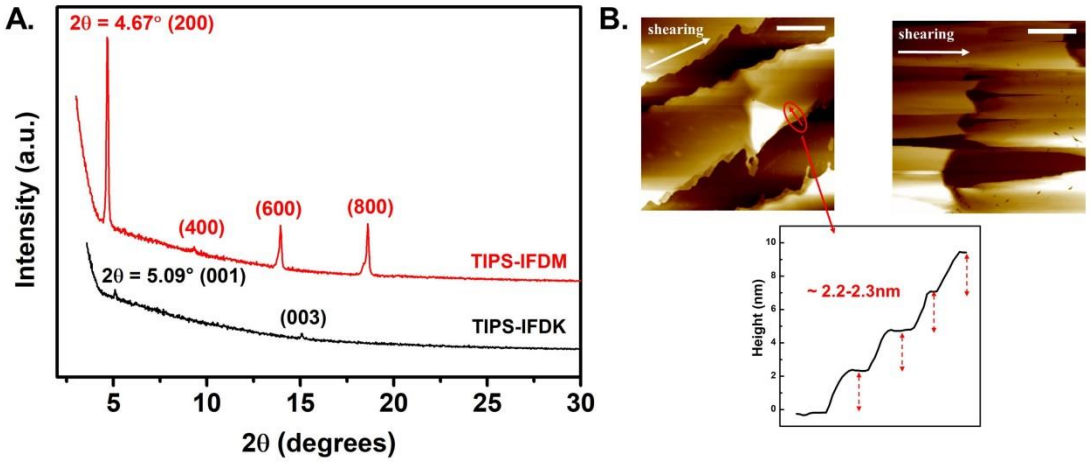

Figure 2.3.3.1. θ-2θ X-ray diffraction (XRD) scans (A) and AFM topographic images (B) of the solution-sheared **TIPS-IFDK** (left) and **TIPS-IFDM** (right) thin-films showing the indexed diffraction peaks based on single-crystal unit cell parameters. Scale bars denote 5 μm. White arrow shows the shearing direction and red arrow shows the direction of step-height profile.

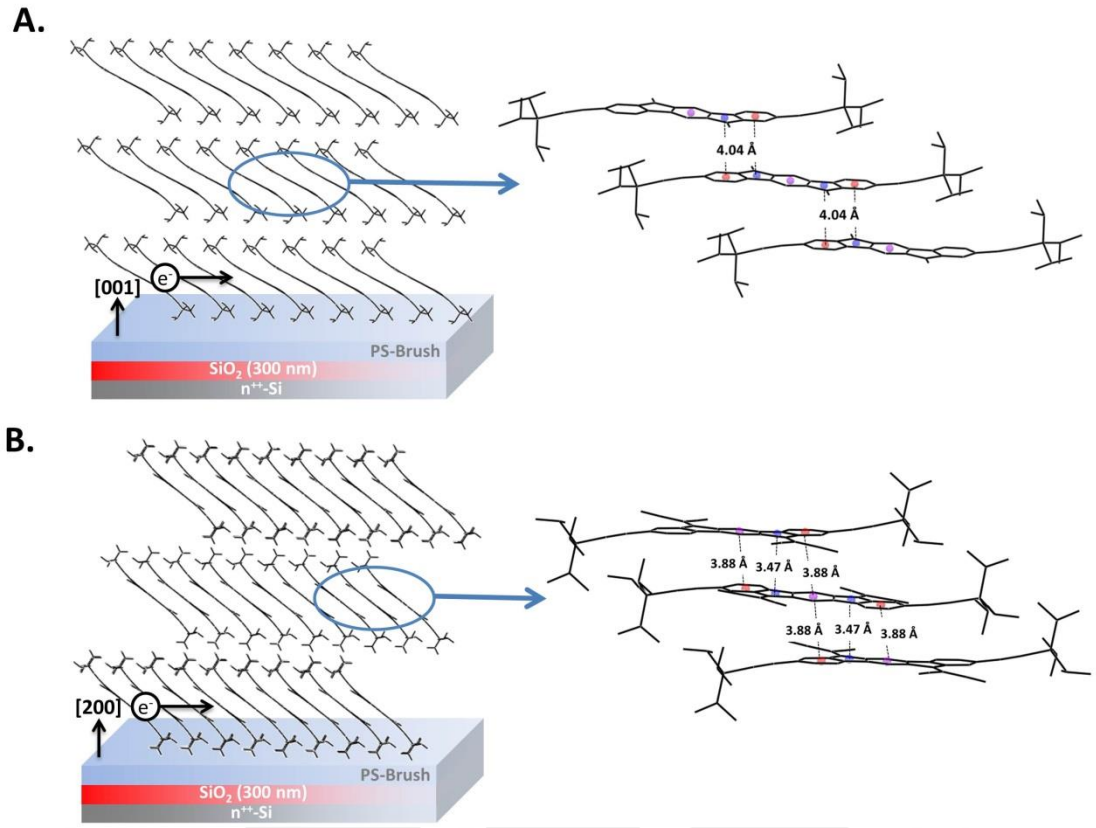

Figure 2.3.3.2. The molecular arrangements in the out-of-plane 001 and 200 directions in **TIPS-IFDK** (A) and **TIPS-IFDM** (B) thin-films showing intermolecular π-π interactions and stacking distances between neighboring molecules in the charge-transport direction.

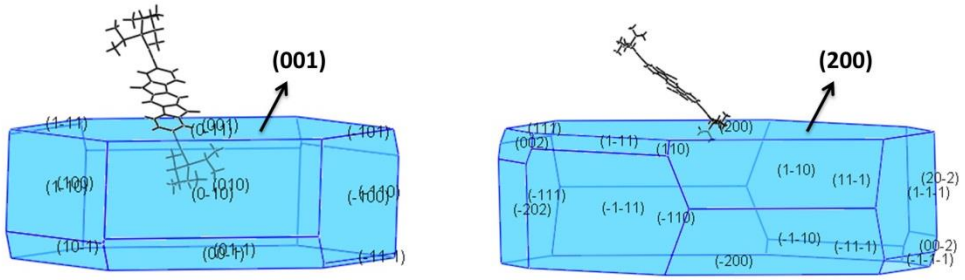

TIPS-IFDK **TIPS-IFDM**

Figure 2.3.3.3 The BFDH (Bravais, Friedel, Donnay and Harker) theoretical crystal morphologies for **TIPS-IFDK** and **TIPS-IFDM** showing the XRD-based observed (001) and (200) crystal planes

The semiconductor characteristics of the present small molecules were measured in top-contact/bottom-gate (TC-BG) OFET devices. Au source-drain electrodes were deposited on solution-sheared TIPS-IFDK(M)/PS(polystyrene)-brush/SiO_2(300 nm)/n^{++}-Si substrates by physical vapor deposition under vacuum (1×10^{-6} Torr). The transistor electrical characterizations were performed both under vacuum and in ambient. Consistent with the theoretical/experimental optoelectronic properties (*vide supra*), the devices exhibited *n*-channel charge-transport characteristics. Typical transfer plots are shown in Figure 2.3.3.4. **TIPS-IFDM** devices showed electron mobility as high as 0.02 cm^2/Vs with an impressive I_{on}/I_{off} ratios of 10^7-10^8 and threshold voltage of ca. 2 V in ambient. To the best of our knowledge, this molecule is the first example of a solution-processable, ambient-stable *n*-type molecular semiconductor functionalized with (trialkylsilyl)ethynyl groups along the long molecular axis. In contrary to the prior reports in the literature showing 1-D slipped-stacked molecular systems lead to poor mobilities ($<10^{-3}$-10^{-4} cm^2/Vs), here we observed an appreciable mobility thanks to the presence of strong π-π interactions along these one-dimensional channels. However, when the π-π interactions along these channels become less effective (*vide supra*) and the overall film crystallinity is lowered in **TIPS-IFDK**-based films, charge-transport performance significantly drops resulting in three orders of magnitude lower electron mobility ($\mu_e = 4\times10^{-5}$ cm^2/Vs, I_{on}/I_{off} = 10^3-10^4, V_{TH} = ca. 30 V) in the corresponding OFETs. While highly stabilized LUMO energy level (-4.18 eV) of **TIPS-IFDM** allows for ambient stable electron-transport, **TIPS-IFDK**-based OFETs showed device activity only under vacuum as a result of its relatively high-energy LUMO (-3.65 eV). It is noteworthy that the *p*-channel semiconductivity previously observed with the reference thienyl-substituted semiconductor, **β-DD-TIFDKT**, is completely nonexistent in **TIPS-IFDK**. This could be ascribed to the absence of thienyl donor units in the new acceptor-type molecule and its stabilized HOMO energy level (-5.77 eV *vs* -5.62 eV for **β-DD-TIFDKT**). Our results clearly show that dicyanovinylene functionalization in indenofluorenes yields efficient π-π stackings, and **IFDM** π-core is a proper-sized, favorable acceptor unit for building (trialkylsilyl)ethynyl-substituted solution-processable, ambient-stable *n*-type semiconductors. We believe that further structural optimizations on –R substituents and R_3Si-C≡C- substitution positions in indenofluorene π-

systems could yield two-dimensional packing motifs in the solid-state and improve charge carrier mobilities.

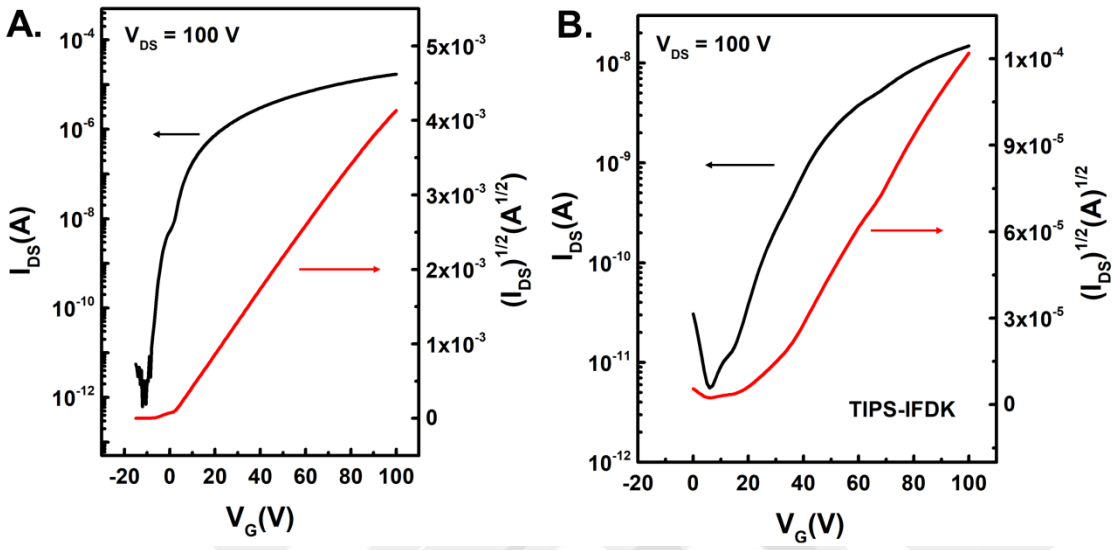

Figure 2.3.3.4. Representative transfer curves in the *n*-channel region for Au/semiconductor/PS(polystyrene)-brush/SiO_2(300 nm)/n^{++}-Si top-contact/bottom-gate (TC-BG) OFET devices fabricated with solution-sheared **TIPS-IFDM** (A) and **TIPS-IFDK** (B) thin-films.

Chapter 3

Conclusions and Future Prospects

3.1 Conclusions

The scope of this thesis includes the design, synthesis, full characterization, single-crystal structures, optoelectronic properties, solution-processed thin-film morphologies/microstructures, and *n*-channel field-effect responses of two novel solution-processable molecular semiconductors **TIPS-IFDK** and **TIPS-IFDM**. These molecular structures are designed bearing (triisopropylsilyl)ethynyl end units at 2,8-positions of highly electron-deficient, ladder type indeno[1,2-b]fluorene-6,12-dione (**IFDK**) and indeno[1,2-b]fluorene-6,12-bis(dicyanovinylene) **(IFDM)** π-cores. As a result of having fully acceptor type π-backbones, when compared with previously developed donor-acceptor type indenofluorenes, both HOMO/LUMO energies of the new compounds (-5.77/-3.65 eV for **TIPS-IFDK** and -5.84/-4.18 eV for **TIPS-IFDM**) were found to be lower resulting in slightly increased optical band gaps of 2.12 eV for **TIPS-IFDK** and 1.66 eV for **TIPS-IFDM**. DFT calculations revealed the electronic effects of (triisopropylsilyl)ethynyl substitutions on frontier molecular orbitals; (triisopropylsilyl)ethynyl's effect on LUMO is mostly through inductive effect while it is a part of the HOMO topography. Single-crystal X-ray diffraction (XRD) analysis revealed highly coplanar structures for the central **IFDK/IFDM** cores, and slightly S-shaped molecular frameworks. Although both semiconductors exhibit very similar slipped 1-D columns in the solid-state, **TIPS-IFDM** molecules showed significant degree of π-π stackings (3.47 Å) that involves the whole indenofluorene π-framework while **TIPS-IFDK** showed much limited intermolecular π-π

interactions with increased (4.04 Å) stacking distances. This shows that although the general solid-state ordering motif is governed by the entire molecular frameworks, which are exactly the same for both molecules, interactions between adjacent molecules is highly influenced by functional groups (carbonyl *vs* dicyanovinylene). Top-contact/bottom-gate OFETs fabricated via solution-shearing **TIPS-IFDM** solution has yielded *n*-channel devices with an ambient-stable electron mobility of 0.02 $cm^2(V\ s)^{-1}$ and I_{on}/I_{off} ratios of 10^7. To the best of our knowledge, this is the first example of solution-processable, ambient-stable *n*-type molecular semiconductor functionalized with (trialkylsilyl)ethynyl groups along the long molecular axis. Detailed microstructural and morphological analysis of the corresponding solution-sheared semiconductor films reveals that **TIPS-IFDM** molecules orient on the surface having (200) crystal plane parallel to the substrate surface, which allows the formation of 1-D slipped π-π stacks along the charge-transport direction. Atomic force microscopy characterizations of the present semiconductor thin-films showed the formation of micrometer-sized ribbon-like domains aligned along the shearing directions. The surface of these ribbons appear to be very smooth over micrometer-sized areas indicating highly favorable two-dimensional molecular coverage grown via *layer-by-layer* mechanism on the surface during the solution-shearing process. As a result of less effective π-π interactions and the poor crystallinity in thin-film phase, **TIPS-IFDK** showed three orders of magnitude lower electron mobility.

In conclusion, our results clearly show that dicyanovinylene functionalization in solution-processable (trialkylsilyl)ethynyl-substituted indenofluorenes yields efficient π-π stackings. **IFDM** π-core is found to be a proper-sized, favorable acceptor unit for building (trialkylsilyl)ethynyl-substituted solution-processable, ambient-stable *n*-type semiconductors. In contrast to the previous design approaches embedding (trialkylsilyl)ethynyl substitutitions along short molecular axis, the current design demonstrates that long molecular axis could be a highly favorable substitution position for high-performance semiconductors. Our findings clearly provide a new molecular design approach for the preparation of solution-processable small molecules as ambient-stable *n*-type semiconductors for organic field-effect transistors and potentially various organic (opto)electronic technologies.

3.2 Future Prospects

On the basis of significant findings presented in this thesis, we envision that further structural optimizations on –R substituents and R_3Si-C≡C- substitution positions in indenofluorene π-systems could yield two-dimensional packing motifs in the solid-state and improve charge carrier mobilities. To this end, the effects of shorter (methyl and ethyl) and longer (tert-butyl) alkyl substituents, and also switching to short molecular axis positions could be studied by designing new molecular structures. Thiophene and thiazole offers great advantages as potential donor units that could be placed adjacent to the indenofluorene core structure. Considering that electron mobility decreased as a result of removing thiophene donor units, further studies could also involve the synthesis of new (trialkylsilyl)ethynyl-substituted donor-acceptor-donor small molecules with thiophene(thiazole) donor units and IFDK(IFDM) acceptor units. These molecular structures could yield much improved charge carrier mobilities, and enable ambipolar charge transport as well. Moreover, designing new structures in this family would be very important to better understand relationships between molecular structures, (opto)electronic properties, and device electrical performance. Finally, device performances could be further optimized by using various device structures (i.e. bottom-gate/bottom-contact (BG/BC), and top-gate coplanar or staggered), dielectric materials (i.e. Al_2O_3, and Polyvinyl alcohol (PVA)), and film deposition techniques (i.e. spin-coating and drop-casting). We strongly believe that our findings in this thesis will open a new door for future realization of solution-processable molecular semiconductor families that could be synthesized in a few synthetic steps.

BIBLIOGRAPHY

1. Kraft, A., Grimsdale, A. C. & Holmes, A. B. Electroluminescent Conjugated Polymers - Seeing Polymers in a New Light. *Angew. Chemie - Int. Ed.* **37,** 402–428 (1998).

2. Reese, C. & Bao, Z. Organic single-crystal field-effect transistors. *Mater. Today* **10,** 20–27 (2007).

3. Burroughes, J. H. *et al.* Light-emitting diodes based on conjugated polymers. *Nature* **347,** 539–541 (1990).

4. Yu, G., Gao, J., Hummelen, J. C., Wudl, F. & Heeger, A. J. device structure consisted Polymer Photovoltaic Cells : Enhanced Efficiencies via a (Ca The on a g | | g. *Science (80-.).* **270,** 1789–1791 (1995).

5. Hide, F. *et al.* Semiconducting Polymers: A New Class of Solid-State Laser Materials. *Science (80-.).* **273,** 1833–1836 (1996).

6. Tessler, N., Denton, G. J. & Friend, R. H. Lasing from conjugated-polymer microcavities. *Nature* **382,** 695–696 (1996).

7. Slinker, J. *et al.* Solid-state electroluminescent devices based on transition metal complexes. *Chem. Commun.* 2392–2399 (2003). doi:10.1039/B304265K

8. Akcelrud, L. Electroluminescent polymers. *Prog. Polym. Sci.* **28,** 875–962 (2003).

9. Pierret, R. F. Semiconductor Device Fundamentals. *New York* 792 (1996). doi:10.1007/BF00198606

10. Mei, J., Kim, D. H., Ayzner, A. L., Toney, M. F. & Bao, Z. Siloxane-terminated solubilizing side chains: Bringing conjugated polymer backbones closer and boosting hole mobilities in thin-film transistors. *J. Am. Chem. Soc.* **133,** 20130–20133 (2011).

11. Fridman. Simultaneous polymerization and formation of polyacetylene film on the surface of concentrated soluble Ziegler-type catalyst solution. *J. Polym. Sci. - Polym. Chem. Ed.* **12,** 11–20 (1974).

12. Chiang, C. K. *et al.* Electrical conductivity in doped polyacetylene. *Phys. Rev. Lett.* **39,** 1098–1101 (1977).

13. Facchetti, A. Semiconductors for organic transistors. *Mater. Today* **10,** 28–37 (2007).

14. Clemens, W., Fix, W., Ficker, J., Knobloch, A. & Ullmann, A. From polymer transistors toward printed electronics. *J. Mater. Res.* **19,** 1963–1973 (2004).

15. Lee, C.-H., Sazonov, A. & Nathan, A. High-mobility nanocrystalline silicon thin-film transistors fabricated by plasma-enhanced chemical vapor deposition. *Appl. Phys. Lett.* **86,** 222106 (2005).

16. Di, C., Liu, Y., Yu, G. & Zhu, D. Interface Engineering: An Effective Approach toward High-Performance Organic Field-Effect Transistors. *Acc. Chem. Res.* **42,** 1573–1583 (2009).

17. Heeger, A. J. Semiconducting polymers: The third generation. *Chem. Soc. Rev.* **39,** 2354–2371 (2010).

18. Newman, C. R. *et al.* Introduction to Organic Thin Film Transistors and Design of n-Channel Organic Semiconductors. *Chem. Mater.* **16,** 2236–4451 (2004).

19. N. Basescu, Z.-X. Liu, D. Moses, A. J. Heeger, H. N. & N. T. High electrical conductivity in doped polyacetylene. *Nature* **327,** 403–405 (1987).

20. Rahimi, R., Kuchibhatla, S. & Korakakis, D. Effect of dielectric/organic interface properties on charge transport in organic thin film transistors. *J. Appl. Phys.* **113,** 10–14 (2013).

21. Farchioni, R. & G. Grosso. *Organic Electronic Materials*. **41,** (Springer Berlin Heidelberg, 2001).

22. Klauk, H. *Organic Electronics: Materials, Manufacturing and Applications*. *Organic Electronics: Materials, Manufacturing and Applications* (2006). doi:10.1002/3527608753

23. Li, F. M., Nathan, A., Wu, Y. & Ong, B. S. *Organic Thin Film Transistor Integration: A Hybrid Approach*. *Organic Thin Film Transistor Integration: A Hybrid Approach* (2011). doi:10.1002/9783527634446

24. Usta, H. *et al.* Perfluoroalkyl-functionalized thiazole-thiophene oligomers as N-channel semiconductors in organic field-effect and light-emitting transistors. *Chem. Mater.* **26,** 6542–6556 (2014).

25. Scaccabarozzi, A. D. & Stingelin, N. Semiconducting:insulating polymer blends for optoelectronic applications - A review of recent advances. *J. Mater. Chem. A* **2,** 10818–10824 (2014).

26. Martens, S. C., Zschieschang, U., Wadepohl, H., Klauk, H. & Gade, L. H. Tetrachlorinated tetraazaperopyrenes (TAPPs): Highly fluorescent dyes and semiconductors for air-stable organic n-channel transistors and complementary circuits. *Chem. - A Eur. J.* **18,** 3498–3509 (2012).

27. Chua, L. *et al.* General observation of n-type field-effect behaviour in organic semiconductors. *Nature* **434,** 194–199 (2005).

28. Baeg, K. J. *et al.* Charge injection engineering of ambipolar field-effect transistors for high-performance organic complementary circuits. *ACS Appl. Mater. Interfaces* **3,** 3205–3214 (2011).

29. Wang, J., Wang, H., Yan, X., Huang, H. & Yan, D. Organic heterojunction and its application for double channel field-effect transistors. *Appl. Phys. Lett.* **87,** (2005).

30. Zschieschang, U. *et al.* Dinaphtho[2,3-b:2′,3′-f]thieno[3,2-b]thiophene (DNTT) thin-film transistors with improved performance and stability. *Org. Electron. physics, Mater. Appl.* **12,** 1370–1375 (2011).

31. Kumaki, D., Yahiro, M., Inoue, Y. & Tokito, S. Air stable, high performance pentacene thin-film transistor fabricated on SiO2 gate insulator treated with β-phenethyltrichlorosilane. *Appl. Phys. Lett.* **90,** 2005–2008 (2007).

32. Wasikiewicz, J. M. *et al.* Towards solution processable air stable p-type organic semiconductors: Synthesis and evaluation of mono and di-fluorinated pentacene derivatives. *J. Mater. Chem. C* **4,** 7309–7315 (2016).

33. Siegel, J. S. & Wu, Y. *Polyarenes I.* **349,** (Springer Berlin Heidelberg, 2014).

34. Frederickson, C. K., Rose, B. D. & Haley, M. M. Explorations of the Indenofluorenes and Expanded Quinoidal Analogues. *Acc. Chem. Res.* **50,** 977–987 (2017).

35. Oh, J. Do, Kim, D. K., Kim, J. W., Ha, Y. G. & Choi, J. H. Low-voltage pentacene thin-film transistors using Hf-based blend gate dielectrics. *J. Mater. Chem. C* **4,** 807–814 (2015).

36. Subbarao, N. V. V, Gedda, M., Iyer, P. K. & Goswami, D. K. Enhanced environmental stability induced by effective polarization of a polar dielectric layer in a trilayer dielectric system of organic field-effect transistors: A quantitative study. *ACS Appl. Mater. Interfaces* **7,** 1915–1924 (2015).

37. Liu, A. *et al.* Fully solution-processed low-voltage aqueous In2O3 thin-film transistors using an ultrathin ZrOx dielectric. *ACS Appl. Mater. Interfaces* **6,** 17364–17369 (2014).

38. Esro, M., Vourlias, G., Somerton, C., Milne, W. I. & Adamopoulos, G. High-mobility ZnO thin film transistors based on solution-processed hafnium oxide gate dielectrics. *Adv. Funct. Mater.* **25,** 134–141 (2015).

39. Maex, K. *et al.* Low dielectric constant materials for microelectronics. *J. Appl. Phys.* **93,** 8793–8841 (2003).

40. Xu, X. *et al.* Solution-Processed Ambipolar Organic Thin-Film Transistors by Blending p- and n-Type Semiconductors: Solid Solution versus Microphase Separation. *ACS Appl. Mater. Interfaces* **7,** 28019–28026 (2015).

41. Ortiz, P., Facchetti, A. & Marks, T. J. High- k Organic , Inorganic , and Hybrid

Dielectrics for Low-Voltage Organic Field-Effect Transistors. 205–239 (2009).

42. Zaumseil, J. & Sirringhaus, H. Electron and ambipolar transport in organic field-effect transistors. *Chem. Rev.* **107,** 1296–1323 (2007).

43. Lee, W.-H., Wang, C. C. & Ho, J. C. Improved performance of pentacene field-effect transistors using a nanocomposite gate dielectric. *J. Vac. Sci. Technol. B Microelectron. Nanom. Struct.* **27,** 601 (2009).

44. Sirringhaus, H. 25th anniversary article: Organic field-effect transistors: The path beyond amorphous silicon. *Adv. Mater.* **26,** 1319–1335 (2014).

45. Oommen, E. *et al.* IgA antibodies to myeloperoxidase in patients with eosinophilic granulomatosis with polyangiitis (Churg-Strauss). *Clin. Exp. Rheumatol.* **35,** 98–101 (2017).

46. Sirringhaus, H. *et al.* Two-Dimensional Charge Transport in Self-Organized, High-Mobility Conjugated Polymers. *Nature* **401,** 685–688 (1999).

47. Anthony, J. E. Functionalized acenes and heteroacenes for organic electronics. *Chem. Rev.* **106,** 5028–5048 (2006).

48. Payne, M. M., Parkin, S. R., Anthony, J. E., Kuo, C. C. & Jackson, T. N. Organic field-effect transistors from solution-deposited functionalized acenes with mobilities as high as 1 cm2/Vs. *J. Am. Chem. Soc.* **127,** 4986–4987 (2005).

49. Rose, B. D. *et al.* Synthesis, crystal structures, and photophysical properties of electron-accepting diethynylindenofluorenediones. *Org. Lett.* **13,** 2106–2109 (2011).

50. Anthony, J. E., Eaton, D. L. & Parkin, S. R. A road map to stable, soluble, easily crystallized pentacene derivatives. *Org. Lett.* **4,** 15–18 (2002).

51. Sheraw, C. D., Jackson, T. N., Eaton, D. L. & Anthony, J. E. Functionalized pentacene active layer organic thin-film transistors. *Adv. Mater.* **15,** 2009–2011 (2003).

52. Nakagawa, T., Kumaki, D., Nishida, J. I., Tokito, S. & Yamashita, Y. High performance n-Type field-effect transistors based on indenofluorenedione and diindenopyrazinedione derivatives. *Chem. Mater.* **20,** 2615–2617 (2008).

53. Deuschel, W. Fluorenacene und Fluorenaphene. Synthesen in der Indeno-fluorenreihe. II. Endo-cis-Fluorenaphen (Indeno-(2′,1′:1,2)-fluoren) und trans-Fluorenacen (Indeno-(1′,2′:2,3)-fluoren). *Helv. Chim. Acta* **34,** 2403–2416 (1951).

54. Fan, Z. P. *et al.* Boosting the Charge Transport Property of Indeno[1,2-b]fluorene-6,12-dione though Incorporation of Sulfur- or Nitrogen-Linked Side Chains. *Adv. Funct. Mater.* **27,** 1–10 (2017).

55. Usta, H. *et al.* Design, synthesis, and characterization of ladder-type molecules and polymers. air-stable, solution-processable n-channel and ambipolar semiconductors

for thin-film transistors via experiment and theory. *J. Am. Chem. Soc.* **131,** 5586–5608 (2009).

56. Teixeira da Rocha, C. *et al.* Solution Coating of Small Molecule/Polymer Blends Enabling Ultralow Voltage and High-Mobility Organic Transistors. *Adv. Electron. Mater.* **1800141,** 1–9 (2018).

57. Naibi Lakshminarayana, A., Ong, A. & Chi, C. Modification of acenes for n-channel OFET materials. *J. Mater. Chem. C* **6,** 3551–3563 (2018).

58. Maliakal, A., Raghavachari, K., Katz, H., Chandross, E. & Siegrist, T. Photochemical stability of pentacene and a substituted pentacene in solution and in thin films. *Chem. Mater.* **16,** 4980–4986 (2004).

59. Dong, H., Fu, X., Liu, J., Wang, Z. & Hu, W. 25th Anniversary Article: Key Points for High-Mobility Organic Field-Effect Transistors. *Adv. Mater.* **25,** 6158–6183 (2013).

60. Ward, J. W., Lamport, Z. A. & Jurchescu, O. D. Versatile organic transistors by solution processing. *ChemPhysChem* **16,** 1118–1132 (2015).

61. Jiang, J., Kaafarani, B. R. & Neckers, D. C. Design, Synthesis, and Properties of New Derivatives of Pentacene. *J. Org. Chem.* **71,** 2155–2158 (2006).

62. Bénard, C. P., Geng, Z., Heuft, M. A., VanCrey, K. & Fallis, A. G. Double Diels-Alder strategies to soluble 2,9- and 2,9,6,13- tetraethynylpentacenes, photolytic [4 + 4] cycloadditions, and pentacene crystal packing. *J. Org. Chem.* **72,** 7229–7236 (2007).

63. Wang, Y. M., Fu, N. Y., Chan, S. H., Lee, H. K. & Wong, H. N. C. Synthesis, characterization, and reactions of 6,13-disubstituted 2,3,9,10-tetrakis(trimethylsilyl)pentacene derivatives. *Tetrahedron* **63,** 8586–8597 (2007).

64. Azzaroni, O. Polymer brushes here, there, and everywhere: Recent advances in their practical applications and emerging opportunities in multiple research fields. *J. Polym. Sci. Part A Polym. Chem.* **50,** 3225–3258 (2012).

65. Park, S. H. *et al.* A polymer brush organic interlayer improves the overlying pentacene nanostructure and organic field-effect transistor performance. *J. Mater. Chem.* **21,** 15580–15586 (2011).

66. Dharmapurikar, S. S., Arulkashmir, A., Das, C., Muddellu, P. & Krishnamoorthy, K. Enhanced hole carrier transport due to increased intermolecular contacts in small molecule based field effect transistors. *ACS Appl. Mater. Interfaces* **5,** 7086–7093 (2013).

67. Giri, G. *et al.* Tuning charge transport in solution-sheared organic semiconductors using lattice strain. *Nature* **480,** 504–508 (2011).

68. Liu, Z., Becerril, H. A., Roberts, M. E., Nishi, Y. & Bao, Z. Experimental study and

statistical analysis of solution-shearing processed organic transistors based on an asymmetric small-molecule semiconductor. *IEEE Trans. Electron Devices* **56,** 176–185 (2009).

69. Diao, Y., Shaw, L., Bao, Z. & Mannsfeld, S. C. B. Morphology control strategies for solution-processed organic semiconductor thin films. *Energy Environ. Sci.* **7,** 2145–2159 (2014).

70. Ozdemir, M. *et al.* Design, synthesis, and characterization of α,ω-disubstituted indeno[1,2-b]fluorene-6,12-dione-thiophene molecular semiconductors. Enhancement of ambipolar charge transport through synthetic tailoring of alkyl substituents. *RSC Adv.* **6,** 212–226 (2016).

71. Ozdemir, R. *et al.* A Solution-Processable Liquid-Crystalline Semiconductor for Low-Temperature-Annealed Air-Stable N-Channel Field-Effect Transistors. *ChemPhysChem* **18,** 850–861 (2017).

72. Ozdemir, R. *et al.* Ultralow bandgap molecular semiconductors for ambient-stable and solution-processable ambipolar organic field-effect transistors and inverters. *J. Mater. Chem. C* **5,** 2368–2379 (2017).

73. Suzuki, A. Recent advances in the cross-coupling reactions of organoboron derivatives with organic electrophiles, 1995-1998. *J. Organomet. Chem.* **576,** 147–168 (1999).

74. Johansson Seechurn, C. C. C., Kitching, M. O., Colacot, T. J. & Snieckus, V. Palladium-catalyzed cross-coupling: A historical contextual perspective to the 2010 nobel prize. *Angew. Chemie - Int. Ed.* **51,** 5062–5085 (2012).

75. Carmichael, D., Lefloch, P., Legoff, X. F., Piechaczyk, O. & Seeboth, N. Double friedel-crafts acylation reactions on the same ring of a metallocene: Synthesis of a 2,5-diacetylphospharuthenocene. *Chem. - A Eur. J.* **16,** 14486–14497 (2010).

76. Simón, L. & Goodman, J. M. DFT study on the factors determining the enantioselectivity of friedel-crafts reactions of indole with N-acyl and N-tosylimines catalyzed by BINOL-phosphoric acid derivatives. *J. Org. Chem.* **75,** 589–597 (2010).

77. Thirion, D., Poriel, C., Rault-Berthelot, J., Barrière, F. & Jeannin, O. (2,1-a)-Indenofluorene derivatives: Syntheses, X-ray structures, optical and electrochemical properties. *Chem. - A Eur. J.* **16,** 13646–13658 (2010).

78. Li, S. *et al.* Synthesis and Structure of a Functionalized [9]Cycloparaphenylene Bearing Three Indeno[2,1-a]fluorene-11,12-dione-2,9-diyl Units. *Org. Lett.* **19,** 4078–4081 (2017).

79. Anthony, J. E., Brooks, J. S., Eaton, D. L. & Parkin, S. R. Functionalized pentacene: Improved electronic properties from control of solid-state order [20]. *J. Am. Chem. Soc.* **123,** 9482–9483 (2001).

80. Zhang, L. *et al.* Bistetracene: An air-stable, high-mobility organic semiconductor with extended conjugation. *J. Am. Chem. Soc.* **136,** 9248–9251 (2014).

81. Granger, D. B. *et al.* Synthesis and Electrical Properties of Derivatives of 1,4-bis(trialkylsilylethynyl)benzo[2,3-b:5,6-b′]diindolizines. *Org. Lett.* **18,** 6050–6053 (2016).

82. Jung, S. *et al.* A TIPS-TPDO-tetraCN-Based n-Type Organic Field-Effect Transistor with a Cross-linked PMMA Polymer Gate Dielectric. *ACS Appl. Mater. Interfaces* **8,** 14701–14708 (2016).

83. Nicolas, Y. *et al.* TIPS-triphenodioxazine versus TIPS-pentacene: Enhanced electron mobility for n-type organic field-effect transistors. *Org. Electron. physics, Mater. Appl.* **13,** 1392–1400 (2012).

84. Usta, H., Facchetti, A. & Marks, T. J. Air-Stable, Solution-Processable n -Channel and Ambipolar Semiconductors for Thin-Film Transistors Based on the Indenofluorenebis(dicyanovinylene) Core. *J. Am. Chem. Soc.* **130,** 8580–8581 (2008).

85. Zhang, L. *et al.* Bistetracene: An air-stable, high-mobility organic semiconductor with extended conjugation. *J. Am. Chem. Soc.* **136,** 9248–9251 (2014).

86. Kato, T., Uchida, J., Ichikawa, T. & Sakamoto, T. Functional Liquid Crystals towards the Next Generation of Materials. *Angew. Chemie - Int. Ed.* **57,** 4355–4371 (2018).

87. Iino, H., Usui, T. & Hanna, J.-I. Liquid crystals for organic thin-film transistors. *Nat. Commun.* **6,** 6828 (2015).

88. Sheldrick, G. M. SHELXT - Integrated space-group and crystal-structure determination. *Acta Crystallogr. Sect. A Found. Crystallogr.* **71,** 3–8 (2015).

89. Sheldrick, G. M. Crystal structure refinement with SHELXL. *Acta Crystallogr. Sect. C Struct. Chem.* **71,** 3–8 (2015).

90. Spek, A. L. Structure validation in chemical crystallography. *Acta Crystallogr. Sect. D Biol. Crystallogr.* **65,** 148–155 (2009).

91. Spek, A. L. PLATON SQUEEZE: A tool for the calculation of the disordered solvent contribution to the calculated structure factors. *Acta Crystallogr. Sect. C Struct. Chem.* **71,** 9–18 (2015).

92. Macrae, C. F. *et al.* Mercury: Visualization and analysis of crystal structures. *J. Appl. Crystallogr.* **39,** 453–457 (2006).

93. CIF deposition and validation service. Available at: https://www.ccdc.cam.ac.uk/deposit.

94. Becerril, H. A., Roberts, M. E., Liu, Z., Locklin, J. & Bao, Z. High-performance

organic thin-film transistors through solution-sheared deposition of small-molecule organic semiconductors. *Adv. Mater.* **20,** 2588–2594 (2008).

95. Chen, J., Martin, D. C. & Anthony, J. E. Morphology and molecular orientation of thin-film bis(triisopropylsilylethynyl) pentacene. 1701–1709 (2007). doi:10.1557/JMR.2007.0220